QUANTIFICATION OF CHRONIC MICROELECTRODE SIGNAL QUALITY OVER TIME

by

Trevor W Sleight

Bachelor of Science in Engineering, Geneva College, 2008

Submitted to the Graduate Faculty of

Swanson School of Engineering in partial fulfillment

of the requirements for the degree of

Master of Science

University of Pittsburgh

2010

UNIVERSITY OF PITTSBURGH

SWANSON SCHOOL OF ENGINEERING

This thesis was presented

by

Trevor W Sleight

It was defended on

March 23, 2010

and approved by

Dr. Tracy Cui, Assistant Professor, Department of Bioengineering

Dr. Daniel Simons, Professor, Departmental of Neurobiology

Dr. Douglas Weber, Assistant Professor, Departmental of Physical Medicine and Rehabilitation

Thesis Advisor: Dr. Tracy Cui, Assistant Professor, Department of Bioengineering,

Thesis Co-Advisor: Dr. Douglas Weber, Assistant Professor, Departmental of Physical Medicine and Rehabilitation

QUANTIFICATION OF CHRONIC MICROELECTRODE SIGNAL QUALITY OVER TIME

Trevor W. Sleight, M.S.

University of Pittsburgh, 2010

The developing field of brain machine interface contains enormous potential for therapeutic benefit. One of the most direct interfaces is the penetrating microelectrode array. However, the failure of chronically implanted neural probes limits the usefulness of penetrating microelectrodes for human brain machine interfaces. Over the course of several weeks after implantation, neural probes lose their ability to record signals due to a variety of tissue reactions including neuronal loss and glial scarring. Several forms of surface enhancements and drug delivery solutions have been proposed. However, in order to systematically evaluate these techniques, a reliable chronic recording model is needed that can offer quantification of recording quality, longevity and reliability. The results of this study are twofold. We present several parameters that may be used as metrics for quantifying the decay of signal quality in a microelectrode array. Second, we consider the effects of a potential surface modification for improving these parameters. In this study, we characterized the quality of neural recordings obtained from microelectrode arrays (16-channel, NeuroNexus, Inc, 16-channel, MicroProbes for Life Science) implanted chronically in the barrel cortex of adult rats. Signal to noise ratio of unit waveforms, local field potential and the ability of the implants to respond to a variety of stimulation parameters were evaluated as measures of the survival of the probe. L1 is a neural adhesion molecule that can specifically promote neurite outgrowth and neuronal survival.

Previous *in-vitro* studies have suggested that that a surface modification of L1 may be able to increase the neuronal density local to the probe. We compared the signal degradation of L1 modified probes and unmodified probes over eight weeks. The data suggests trends towards improved signal to noise ratio in the L1 coated probes.

TABLE OF CONTENTS

LIST OF FIGURES

1.0 INTRODUCTION

The field of brain machine interface devices (BMI) is rich with possibilities. Notwithstanding the incredible complexity of the human nervous system, many promising experiments have already been conducted. Technologies range from direct control of robots [1-3] to interface devices with computers, to rehabilitation therapies. [4] The shrinking size of computers offers greater levels of computational sophistication at increasingly lower size and weight. Several different types of neural recording technologies exist, each offering different tradeoffs of temporal or spatial resolution, cost, and biological invasiveness. One of the least invasive varieties is electroencephalography (EEG) where electrodes are mounted outside the skin. EEG has a very limited spatial resolution, and biological noise from the body's other electrical sources is high. A middle ground approach is electrocorticography (ECoG) where a floating grid of electrodes is affixed inside the skull, but outside the actual brain tissue. This technology provides a higher spatial resolution then EEG, but at the cost of higher invasiveness, as surgery must be performed to insert the device. At a still more invasive level, penetrating microelectrode arrays are inserted directly into the brain tissue. These arrays contain numerous recording sites, providing a high degree of spatial precision. Their direct contact with the neuronal tissue also provides a high level of temporal resolution. The ability of these probes to resolve signal down to the level of individual neurons provides a powerful tool for the development of precisely controlled BMIs.

The close proximity of microelectrode arrays to the biological signals necessitates a high-quality interface. This determines the amount of corruption that the signal experiences as it passes out of the body and into the machine. The quality of the interface also determines the level of chronic irritation that the implant will cause. In extreme cases the electrode may be destroyed, and even in mild cases the quality of the signal will degenerate as the electrode inflicts damage. The interface also impacts the effective recording field of the electrode. If the interface is poor, the neurons will migrate away from it, weakening the signal. Thus, these electrodes often fail to function reliably in clinically relevant chronic settings, due to glial encapsulation and loss of neurons. Several promising technologies including surface modifications, mechanical compatibility, and local drug delivery have been proposed as potential solutions to this complicated problem. [5]

In order to determine the effect of an improvement in biocompatibility, the proposed solution must demonstrate a measurable improvement in the final output of the device. This final output is the quality of the actual signal acquired from the probe and the information that can be decoded from it. In order for a biocompatibility improvement to be considered effective, the associated BMI device must be able to perform better, longer, or more consistently in some measurable parameter.

For the researcher to be able to improve the electrode to tissue interface, they must be able to determine not only whether their probes are acquiring better or worse signals, but in what way the signals are better or worse and how this is affected by the method of enhancement. At the most basic level, the problem is one of information transfer. The nervous system codes relevant information in the form of neural action potentials. The theory of implantable neural devices is to tap into this information stream and utilize it for device based assistance. Therefore,

any useful neural implant must not only be able to "hear" activity, but be able to distinguish enough features from the signal to decode useful information.

We have developed a small animal model that provides a means of testing the quality of an implant. The model provides detailed information on the signal quality and reliability of several different parameters, allowing the researcher to measure the performance of different improvement technologies in a robust setting. We have evaluated the tissue impedance, as well as several parameters reflected in neural unit recordings and in the local field potential (LFP). These parameters are well established in the literature as standard measures of chronic signal quality. [5-7] In addition we will quantify the ability of the electrode to transfer information regarding a variety of different stimulations applied to the animal. A pilot study involving a surface modification of the protein L1 has been conducted and the recording model was used to consider the effectiveness of this modification on various recording parameters. Throughout this document we will present data that characterizes chronic signal quality, and where possible compare the L1 surface modification with unmodified probes.

1.1 ELECTRODES

Despite the youthfulness of the field of brain recording, a wide variety of different designs for microelectrode arrays have been developed. The microwire electrode was the original design used for neural recordings. [8] Made from insulated tungsten wires, these electrodes are sometimes configured as tetrodes to improve the differentiation of individual cells. The Utah array is a more complicated structure that resembles a spike-mat. The electrode is constructed of

conductive shanks of monocrystaline silicon. The shanks are electrically insulated from each other with a glass compound. [8, 9] The Michigan probe is also silicon based, but uses a complex etching process in order to deposit the traces on the shank. [8, 10] Michigan shanks must be larger in order to accommodate multiple conductive traces; however, the ratio of recording sites to displaced tissue is dramatically lower than with the Utah or microwire arrays because of the ability to record at multiple points along the shank.

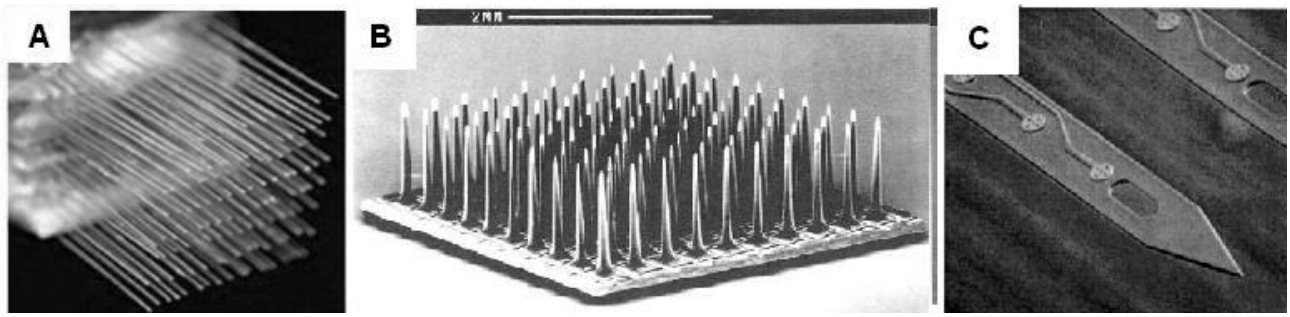

Figure 1: Examples of Different Electrode Designs. (A) Microwire [11] (B) Utah Array [12] (C) Michigan Array [10]

Figure 1 shows examples of different types of electrodes that have been successfully used in research studies. Regardless of the design, the electrodes contain a high density of recording sites. Despite best efforts to minimize the size of the electrode shanks and thereby the damage done to the tissue, it is inevitable that the insertion of any microelectrode will cause significant damage. Future technologies must find ways to minimize the impact of this intrinsic problem.

1.2 TISSUE REACTION

A penetrating electrode poses a difficult challenge in terms of its biocompatibility requirements. The device must be stable relative to the surrounding tissue, which is itself often unstable relative

to nearby tissues. It must be as small as possible in order to minimize the trauma of introducing a foreign object to a biological system, and yet still be sufficiently robust to withstand the aggressive internal environment of the human body. Researchers have found that implanted microelectrodes often lose their ability to record useful signal over time. However, there is a significant degree of variability in the rate and degree of failure of different probes in different settings. [13]

Brain tissue is composed of a complex mixture of different types of cells. In addition to neuronal cells, a wide variety of supporting cells exist to maintain homeostasis and protect the brain from injury. The two primary defensive cells are astrocytes and microglia. Each of these plays a specific, time dependent role in the body's defensive mechanisms. Astrocytes display a characteristic star shape because of their many processes. These cells contain intermediate filaments of glial fibrillary acid protein (GFAP) which is upregulated when the cell is activated by injury. GFAP is commonly used as a cell marker in imaging studies. Microglia are the resident macrophages of the brain and are a major component of the brain's fast response to injury. Microglia typically reside in the brain in a highly branched inactivated state until activated by an injury. [13]

1.2.1 Acute Reaction

There are two phases of tissue reaction to the implantation of an electrode. One is the swift response of inflammation characteristic to an injury at any point in the body. When an electrode is implanted in the brain a complex cascade of biological reactions is triggered. Several different factors contribute to the details of the response. Certain studies suggest that the exact geometry

of the probe can have a significant impact on the details of the acute response, although the chronic response is minimally impacted. [14] Most electrodes are designed to come to a sharp point at the tip, allowing them to cut a hole in the tissue as they are inserted. Despite efforts to minimize the scope of the trauma, tissue in the immediate area of each shaft will experience some degree of compression and tearing, causing damage local to the implant site.

In response to the injury of the brain tissue, microglia are activated and proliferate into macrophages, correlating with inflammation and the body's swift reaction to an injury. In addition, microglia release cytotoxins and pro-inflammatory factors such as TNF-α and MCP-1. If blood vessels are broken by the implant, macrophages from the bloodstream will also be present. Damaged and destroyed tissue is removed by phagocytosis. [13, 15, 16]

1.2.2 Impedance and Chronic Glial Scaring

The chronic glial response is a unique feature of the central nervous system's defensive mechanism. As the inflammation of the acute response dies down, astrocytes interlock into a dense matrix encapsulating the probe. This sheath is implicated in many of the problems that occur in chronic microelectrodes. Following injury, astrocytes up-regulate the expression of glial fibrillary acidic protein (GFAP). These cells form a dense sheath ranging from 50 to 100 μm, and with an increased presence of GFAP positive reactive cells up to 500 μm from the implant site. [13] Since the effective reliable range of a recording electrode is approximately 50 μm (depending on the electrode and exact context) this is a significant problem for chronic recordings.

The impedance of a recording electrode is another important parameter for neural recording. The gradual increase of impedance due to encapsulation tissue and scaring is a well established phenomenon. [17] The details of how this increase impacts the ability of a chronically implanted microelectrode to continue to provide useful signal over a long amount of time is somewhat less certain. [5, 18]

1.2.3 Neuronal Survival and Cell Death

At an even more basic level, the death of neurons proximal to the implantation site has a profound impact on the presence and clarity of neuronal signal. There is considerable evidence that the insertion of a microelectrode into brain cortex causes a "kill zone" of decreased neuronal density immediately surrounding the electrode. The exact dimensions of the kill zone depend on the severity of the tissue reaction and much of this dead zone is created during the acute response. One study found that as early as 2 weeks, reduced neuronal density was found up to 230 μm from the probe surface. Many explanted neuronal probes still had macrophages attached to them, suggesting that the immediate area surrounding the probe was still under some level of inflammation, making it an unattractive environment for neuron outgrowth. [16]

1.3 CHRONIC NEURAL SIGNAL

1.3.1 Signal Degradation over Time

The aggressive internal environment in which a neural probe must live tends to result in the degradation of signal quality as the biological reactions either destroy the probe or isolate it from the relevant signals in the brain. However, although it is universally accepted that chronic neural signal quality decays, there is a significant level of variability between different studies regarding how this happens, to what extent, and what the expected time course should be. Nicoleis et al, 2003 observed a 40% decrease in the overall number of channels on which a unit could be isolated over eighteen months, and there were differences depending on the region of the brain. [11] Another study, Lui et al, 1999, found that there was a gradual loss of detectable signal over six months, ultimately resulting in no signal at all. [19] A variety of different time courses of stability were observed. Williams et al, 1999 found that the number of implanted electrodes that were active at least once a week decreased from 90% to 25% over twelve weeks. [20]

1.3.2 Previous Solutions

Several different methods have arisen as possible solutions to this complex problem. Many studies have focused on different methods of modifying the surface of a neural implant in order improve its overall biocompatibility. These techniques include treating the electrode surface with conducting polymers [21] or mounting laminin, and laminin derived molecules on the surface. [22, 23] In addition, there has been significant work towards developing effective drug therapies to reduce the severity of the reaction of the host tissue to the implanted electrode. [24, 25] Other

studies suggest that patterns of electrical current applied to an electrode's recording sites can rejuvenate the sites and improve signal quality. [26, 27]

1.4 SPECIFIC AIMS

Previous studies have quantified a variety of different signal quality parameters. One common measurement is tissue impedance, which is believed to be representative of certain biological features, such as the thickness of the scar sheath. [6, 28-30] Other studies count the number of isolatable neural spiking units over time. [19, 20] Certain measurements provide some details about the strength of the signal. Signal to noise ratio is typically computed as a relationship between the height of the neural spikes and the remainder of the signal. The peak to peak amplitude of the (LFP) is also used as a measure of chronic signal quality. [5, 7]

However, while these measurements provide a useful measure of the strength of the signal and the health of the neural tissue proximal to the implanted probe, they are still a step removed from the most relevant information. In order to function reliably in a clinical setting, a chronic BMI device must be able to reliably decode the same information over an extended period of time. Furthermore, certain aspects of the neural signal, such as multi-unit activity, are important in BMI applications, but do not directly lend themselves to the more common methods of chronic signal analysis. Therefore, the stability of the information carried in a neural signal is what must really be considered in evaluating the quality of a neural interface.

Our recording system allows the delivery of a variety of preciously controlled stimulation. This provides us with a metric for quantifying the stability of the information carried

in a neural signal. The system can fire air puffs to deliver simple whisker deflections, or modulate a series of puffs to deliver a variety of different patterns of sequential stimulation. This provides for different levels in the complexity of the stimulation. Measurements of the stability of the evoked responses can then be correlated with the traditional measures of raw signal quality, providing a more holistic understanding of the performance of the neural interface over time.

2.0 METHODS AND MATERIALS

Two different levels of the experimental design are described here. The experimental design and recording paradigm are novel and provide an unusual look into the details of chronic microelectrode signal quality. Once the recording paradigm was established, it was applied to test the usefulness of a protein surface modification that has previously been shown to increase neuronal density *in-vitro*. [31]

2.1 BARREL CORTEX

The barrel (whisker) cortex of the rat was selected as the experimental model for this study. This portion of the brain is named for the discrete columnar structures in layer IV of the cortex which correspond to each of the individual whiskers and resemble small isolated "barrels." Neural imaging techniques such as intrinsic imaging or voltage sensitive dies have provided high resolution characterization of the barrel cortex in-vivo. [32-34] This area of the brain is rich with histological and informational potential and provides a good model for testing the effect of biocompatibility enhancements to chronic microelectrodes. The complexity of the inter-barrel circuitry allows the rat to both to discriminate between surface textures of different objects, and also to precisely locate a touched object in space. [33, 35] Much of this information processing

appears to occur at the cortical level, with different cortical layers performing different types of signal integration or separation. The potential for detailed signal analysis makes this portion of the brain an information rich area for neural recording.

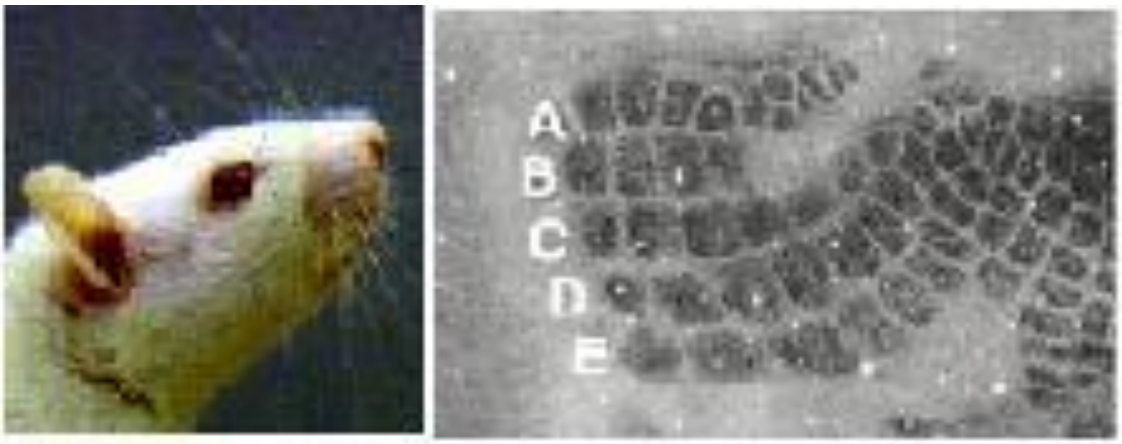

Figure 2: Layer IV of the Barrel Cortex. Individual "barrels" composed of glial cells, excitatory spiny stellate cells and inhibitory interneurons. Each barrel receives input from one primary whisker. (Image Credit (http://simonslab.neurobio.pitt.edu/)

Figure 2 shows an image of Layer IV which is often the primary target of extracellular recordings in barrel cortex. This layer contains distinct structures corresponding to each whisker. Exhibiting a roughly circular morphology, these dense arraignments are termed "barrels" and the intervening space is termed "septa". The barrels are laid out in a structure similar to the arraignment of the whiskers on the rat's face.

The structured morphology of the barrel cortex is reflected at several stages in the information processing chain. Much of the somatosensory signal passes from the sensory neurons through the brainstem and the thalamus, and finally to the somatosensory cortex. In the case of the rat vibrissa, the trigeminal nucleus of the brainstem contains structures called "barrrelettes", which each correspond to a single whisker. Principle trigeminal neurons project

from to the ventral posterior medial nucleus (VPM) which contains structures called "barreloids". The axons from these barreloids project to layer IV of the barrel cortex in the somatosensory cortex. [33, 36]

Information enters the barrel cortex through two primary thalamic pathways. The lemniscal inputs arise from the VPM. These inputs carry information about passive whisker deflections to the barrels in layer IV and Vb. The paralemniscal inputs come from the postermedial nucleus of the thalamus (POM). The POM projects primarily to layers I and Va of the barrel cortex. [37] Paralemniscal inputs contain information about the location of whiskers in space, incorporating sensorimotor information from active whisking. The inter-barrel septa receive input from both thalamic sources. [38, 39] Recently, a third pathway, termed the extralemiscal pathway has also been suggested. This pathway projects from the paralemniscal nuclei in the ventrolateral sector of the VPM to layer IV and carries information about whisker contact with objects. [38, 39]

Layer IV is often referred to as the granular layer because of the discrete grain-like appearance of the cells under Nissel staining. However, Golgi staining revealed the presence of spiny stellate cells in layer IV. [40] In addition to glial cells, each individual barrel column is composed of excitatory principle neurons (75-85%) and inhibitory interneurons (12-25%). [38] The layer IV spiny neurons receive input from the VPM projections and are considered the primary element in intracortical signal processing, and therefore these cells are the most likely source of most microelectrode recordings. [37]

Little consideration is given to layer I. This layer is contains many lateral projections, and minimal processing occurs here. Layers II and III of the barrel cortex are typically combined and discussed as a single layer (layer II/III). Much of the integral processing for combining

information from multiple whiskers occurs in layer II/III. [37] Layers II and III of the barrel cortex are referred to as the subgranular layers and V-VI are termed the infragranular layers. Figure 3 provides a histological example of the different layers.

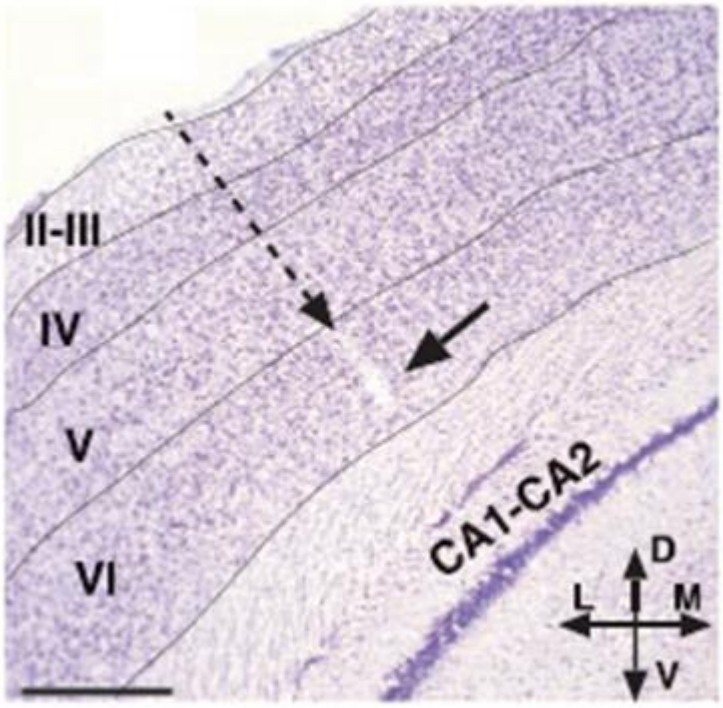

Figure 3: Histological Layers of the Barrel Cortex. Arrows indicate a lesion. [41]

The different layers and different pathways display distinct characteristics in the overall information processing scheme. The inter-barrel septal circuitry is more responsive to the rate of stimulation, providing information about the type of object that a rat may be encountering. Conversely, the barrel structures code spatiotemporal information related to the locations of objects in time and space. [35, 42] The breadth of different types of signals that can be recorded makes the barrel cortex an ideal model for the evaluation of chronic signal quality.

2.2 EXPERIMENTAL DESIGN

2.2.1 Surgical Procedures for Neural Implants

Adult male Sprague-Dawley rats were used throughout this study. The animals were housed in the facilities of the University Of Pittsburgh Department Of Laboratory Animal Resources and given free access to food and water. All experimental protocols were approved by the university Institutional Animal Care and Use Committee. The implanting techniques were followed as previously described by Vetter et al. [43] The probes were implanted in the barrel cortex of the animal. General anesthesia was achieved in 5 min with a mixture of 5% isoflurane and 1 L/min O_2 prior to surgery and maintained throughout the surgical procedure at 1-3% isoflurane. The state of anesthesia was closely monitored for changes in reduction of respiratory rate, heart rate, and the absence of the pedal reflex. The animal was placed into a stereotactic frame and its head was shaven over the incision area. The animal's skin was disinfected with isopropyl alcohol and betadine and a sterile environment was maintained throughout the surgical procedure. Ophthalmic ointment was applied to the eyes to prevent drying from exposure to anesthesia. A midline incision was made along the scalp, the skin retracted, and the periosteum was cleared to expose the bregma and midline. A 2-3mm craniotomy was hand-drilled above the motor cortex (coordinates from bregma: AP: -0.5, ML: ± 2.5-3.5). This provided for a more controlled craniotomy than using an electric drill, which can cause iatrogenic damage. One probe was implanted in the right hemisphere of every rat (L1 and non modified probe). Several stainless steel bone screws were placed in the skull to retain the dental acrylic head-cap. After probe mounting, the dura layer was incised using a fine dura pick (Fine Science Tools). In the case of

the Michigan probe, the bond-pad region of the microelectrode was grasped with Teflon-coated microforceps and the penetrating shank was inserted manually through the pia mater into the barrel cortex. The FMA was inserted with the aid of a micro-manipulator and a homemade suction tool on which the probe was mounted. To minimize bleeding and tissue reaction, surface blood vessels were avoided during insertion. The craniotomy was filled with a biocompatible silicone elastomer (Kwik-Sil, World Precision Instruments, Inc., FL) followed by dental acrylic. The overlying skin was sutured around the dental acrylic head-cap and the animal was allowed to recover under close observation in the surgical room. To minimize variability associated with the surgery, all implants were performed by the same surgeon.

2.2.2 L1 Coating

The first technology for improving the survival of chronic microelectrodes to be tested with this system was a surface enhancement technique where the neural adhesion molecule L1 was affixed to the surface of the probe. L1 is a neural adhesion molecule involved in central nervous system development. It has been shown to specifically promote neurite growth and attachment. [44-48] We anticipated better signal to noise ratio and improved signal longevity from this coating. A full description of the silane chemistry method used to mount L1 on the probe surface is provided in Appendix C.

2.2.3 Overview

The experiment was developed and adjusted over a period of a little over a year. Several modifications were made to the recording system and the analysis techniques to increase

consistency and improve the clarity of the measured parameters. Figure 4 shows where the different data collected falls in the progression of the experiment.

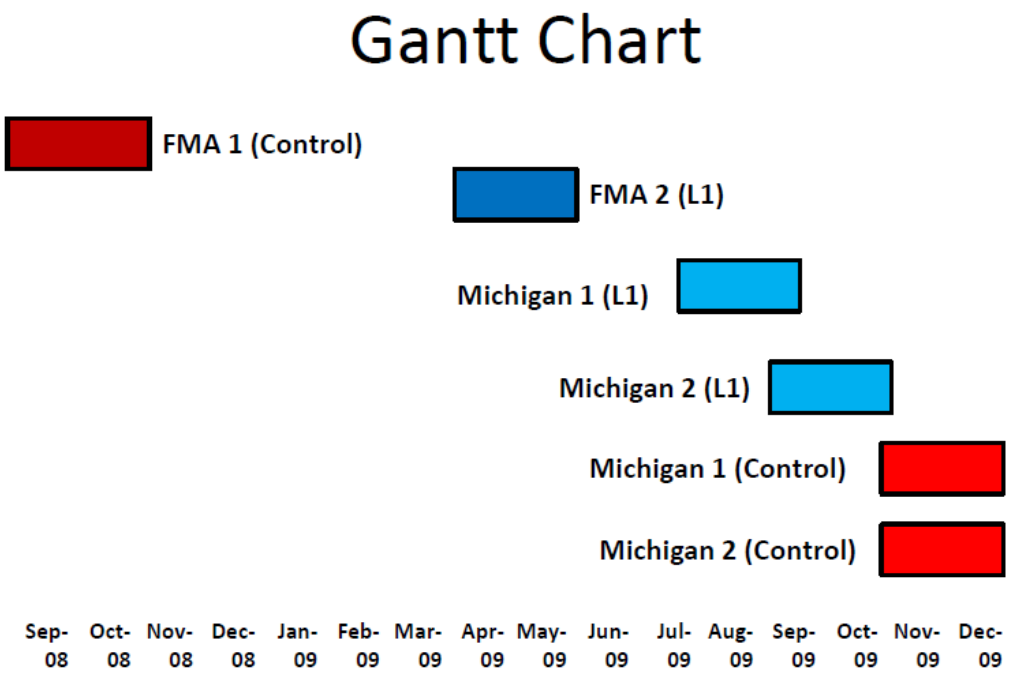

Figure 4: Gantt Chart of Rats. This chart shows when the rat experiments were performed. The major redesign of the recording system (V.1 to V.2) occurred between FMA 1 and FMA 2, and further details were added to the experimental procedure between FMA 2 and Michigan 1.

The experiment was initially conducted with a Floating Microelectrode Array (FMA) (Figure 5.A). Later in the study a single shank Michigan probe was also used (Figure 5.B). The FMA has a better ability to move with the cortex because of flexibility of its anchoring pad. However, the Michigan probe causes less damage during the insertion procedure. The advantages and disadvantages of each probe provided further dynamics to the study.

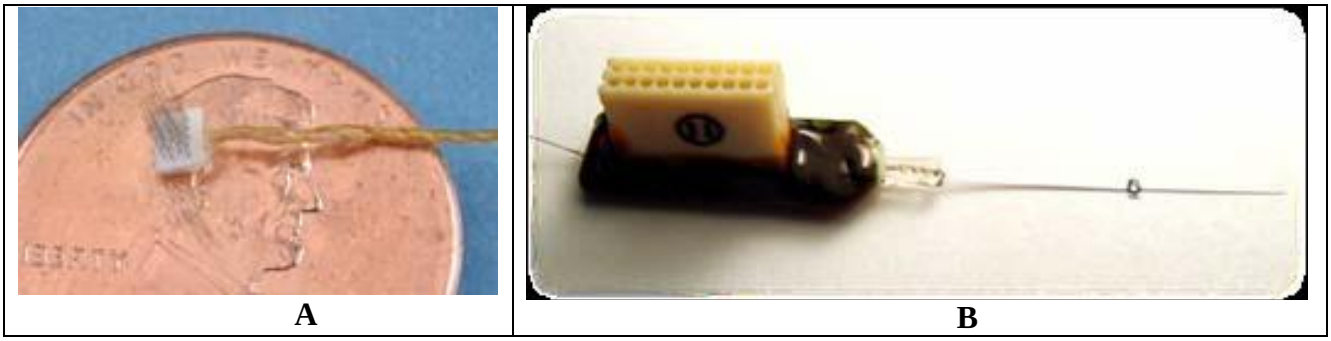

Figure 5: Electrodes Used. (A) Floating Microelectrode Array (MicroProbes for Life Science, Gaithersburg, MD) (B) C-16 Single Shank Michigan Electrode. (NeuroNexus Technologies, Inc. Ann Arbor, MI).

2.3 RECORDING SYSTEM DEVELOPMENT

2.3.1 Pilot Experiments

The initial experiment was conducted without a faraday cage and with the rat awake and behaving. A hand-held air jet was used for stimulation. The researcher allowed the rat to come to a calm rest and then held the jet about three inches away from the rat's face. The rat's whisker pad was divided into 4 quadrants. (A3-C3 by A5-C5, etc) The quadrant bounded by C1-E1 and C3-E3 was selected as the strongest response and used for analysis. The desired stereotaxic location of the stimulus was approximated to the best of the researcher's abilities and air puffs were delivered using a solenoid valve (A valve controlled by an electro-magnetic circuit). This provided a specific input signal that could be translated through the rat's own nervous system and read out again by the probe. Figure 6 illustrates the first recording system.

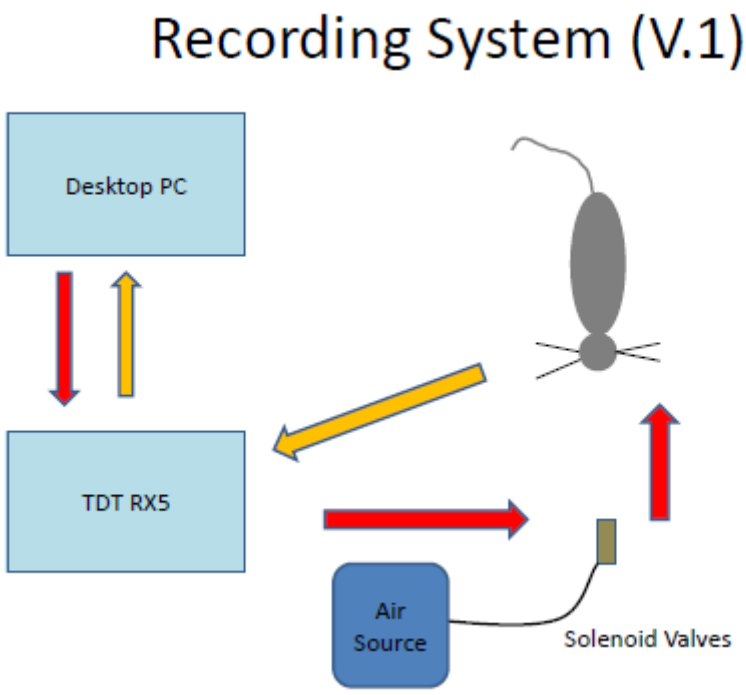

Figure 6. Version 1 of the Recording System. Red lines indicate input information flowing into the rat. Yellow lines indicate output information in the form of neural data obtained from the rat. The stimulus was delivered with an air jet modulated by a solenoid valve and grasped in the researcher's hand. No faraday cage was used, and the experiment was conducted with the rat awake and behaving.

2.3.2 Final Hardware Configuration

In order to increase day-to-day consistency in the recording procedure, it was decided that the experiment would be conducted under general anesthesia. Isoflurane was selected for its ease of use and safety of administration. In addition, a faraday cage was introduced to increase the consistency of environmental background noise, and the configuration of the air jets was improved. More air jets were added and the jets were secured to a micromanipulator suspended over the rat's head (Figure 8). Air pressure was supplied to the solenoid valves through a precision regulator (Control Air Inc. Amherst, NH) at a constant pressure of 20 psi. The jets were

controlled by a solenoid valve (Humphrey, Kalamazoo, MI) which was actuated by a computer through a homemade relay circuit. This allowed precision timing of the air stimulus, as well as pre-programmed stimulation patterns. Generally “puffs” were formed by a 100 ms pulse during which the valve was open. The intervening times during which the valve was closed were adjusted to provide a variety of different frequencies of stimulation.

Recordings were performed twice a week for 8 weeks, usually with 3-4 day intervals. However, only weekly time points were needed for the final analysis, while biweekly recordings provided redundancy. The first week was omitted to allow the rat to recover from the surgery. During a recording procedure anesthesia was induced in the same manner as in surgery, and maintained with 2-2.5% isoflurane. Efforts were made to minimize the depth and duration of the anesthesia, and to keep it consistent between recordings. A passive vacuum hose was used to scavenge waste isoflurane. Isoflurane has a slight suppressive effect on evoked neural activity. [49] However, it was decided that since this effect would be consistent between control and experimental groups, the benefits of simplifying the experiment by the use of anesthesia were worth the tradeoffs of signal quality. Figures 7 provides an outline of the improved system.

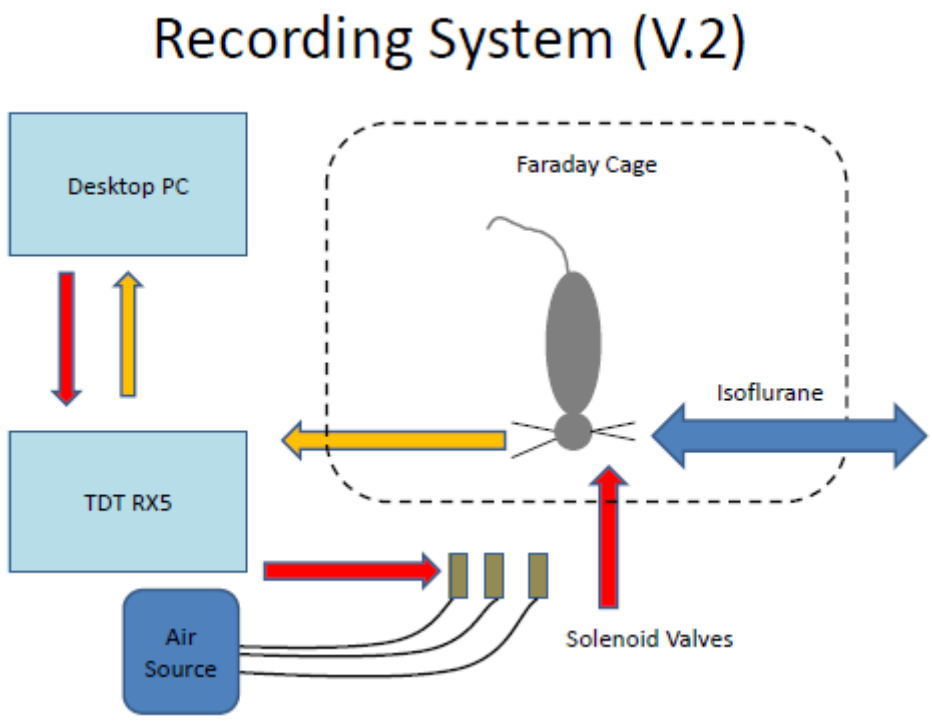

Figure 7: Version 2 of the Recording System. Red lines indicate input information flowing into the rat. Yellow lines indicate output information in the form of neural data obtained from the rat.V.2 added anesthesia (Isoflurane) increased flexibility with the solenoid valves, and a faraday cage.

The recording experiment consisted of several different trials involving a combination of spontaneous recordings where no stimulus was applied, and different paradigms of stimulation to provide the system with a variety of different information to encode and decode. Figure 7 provides an overview of the flow of information. Briefly, spontaneous trials were collected in which no stimulation was applied to the rat. Single shot stimulation was performed by firing several isolated puffs of air on the rat's whiskers from each of the three available air jets individually (Figure 8). The location with the strongest response was considered in the final analysis. Sequential stimulation trials (also termed "Burst" trials) were performed by clicking the solenoid valve for a given jet open and closed at selected frequencies. Impedance measurements

were taken using a Gamry Femtostat (Gamry Instruments Warminster, PA). A skull screw implanted at the back of the skull was used as a reference. The instrument recorded a sweep of data points from 100 kHz to 10 Hz, using six points per decade. A sine wave with an root mean square (RMS) value of 5 mV was used. This provided a range of different frequency measurements.

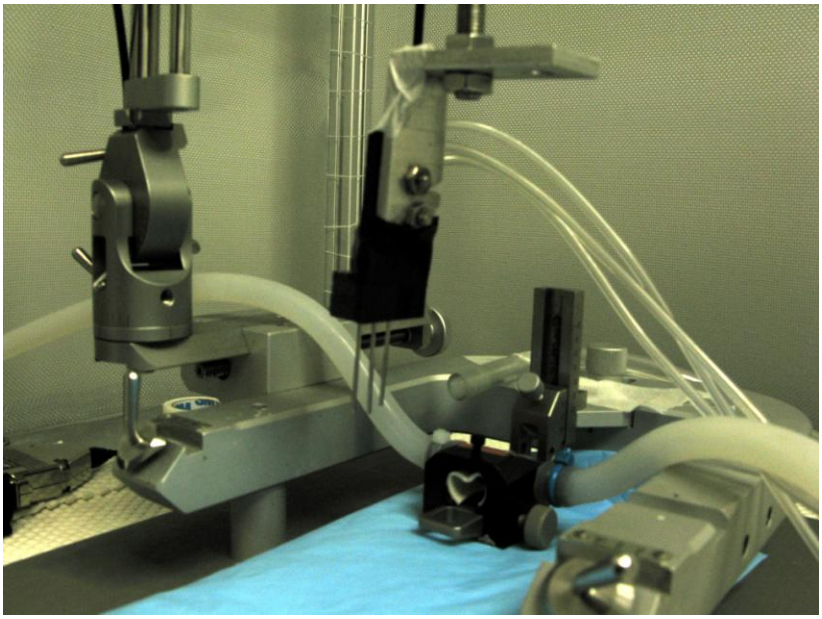

Figure 8: Puffer Apparatus. The three air jets used to simulate the whiskers can be see above the isoflurane mask. The hoses supplying the air enter from the right and the faraday cage insulates the system from environmental noise, as well as the electrical noise of operating the solenoid values. The scavenging hose to collect waste isoflurane can be seen in the back.

The signal was recorded with an RX5 Digitizer, a Medusa Pre-Amplifier and an RA16CH high impedance headstage (Tucker Davies Technologies, Inc, Alachua, FL). The raw signal was sampled at 24414 Hz, and band-pass filtered from 300 Hz to 3000 Hz for single unit recordings. The raw signal was down-sampled to 1017 Hz and band-pass filtered from 1 Hz to 300 Hz for local field potentials. Offline spike detection, sorting, and other analysis were

performed using MatLab (Mathworks Inc, Natick, MA) with custom written programs. See Appendix B for a detailed description of the spike thresholding algorithm. The exact spike count (and therefore the exact firing rate) was often somewhat arbitrary, depending on where the threshold was set, but using this method a rough baseline firing rate can be established, which can then be used to determine the degree of response to stimulus. Snips were sorted using a template algorithm as a guide and then manually inspected for accuracy and the presence of irregular spikes. Due to a problem regarding the Michigan probes, (described below) it was not possible to discern single units on these probes, so only multi-unit activity was considered.

2.3.3 Michigan Signal Problems

The Michigan electrode works by taking the potential difference between the probe's recording sites and a reference located on the probe. It is preferred to use a reference with an impedance of roughly an order of magnitude less than the recording sites. This allows the rejection of the majority of common mode noise. Neural mciroelectrodes also use a grounding wire, which typically has an impedance of about two orders of magnitude below that of the recording sites. Due to an inconsistency in manufacturer documentation, the Michigan probe and the RA16CH headstage were miss-matched and the mapping of the probe's low impedance ground wire and the higher impedance reference site were reversed. This problem was not discovered until late in the study, and consequently, recordings were taken relative to the ground wire rather than relative to the reference site, causing the noise to be somewhat higher than it might otherwise have been had the electrodes been configured correctly. We have elected to analyze this data

anyway because the data still follows some of the expected trends in signal decay. Future experiments will correct this problem.

Because of the problem with the probe reference, we were unable to collect any signals that could truly be considered to be isolatable "single units." However, we have collected a population of snips that we feel represent a combination of single unit and multi-unit activity at a higher time resolution than LFP. Since we cannot determine the exact type of unit described, these signals will hereafter be referred to generically as "snips".

3.0 GENERAL SIGNAL QUALITY PARAMETERS

A significant amount of information can be gained by simply analyzing the quality of a signal without regard to the information that it carries. The characteristics of a signal are often reflective of the quality of the recording site and the success or failure of a surface modification.

3.1 IMPEDANCE

The *in-vivo* impedance of a chronic microelectrode is a critical parameter for recording performance. [6] Ideally, complex impedance can be used to mathematically model different parts of the cellular interactions at the microscopic level. Due to problems with data collection, our recordings were not of sufficient quality to support detailed modeling.

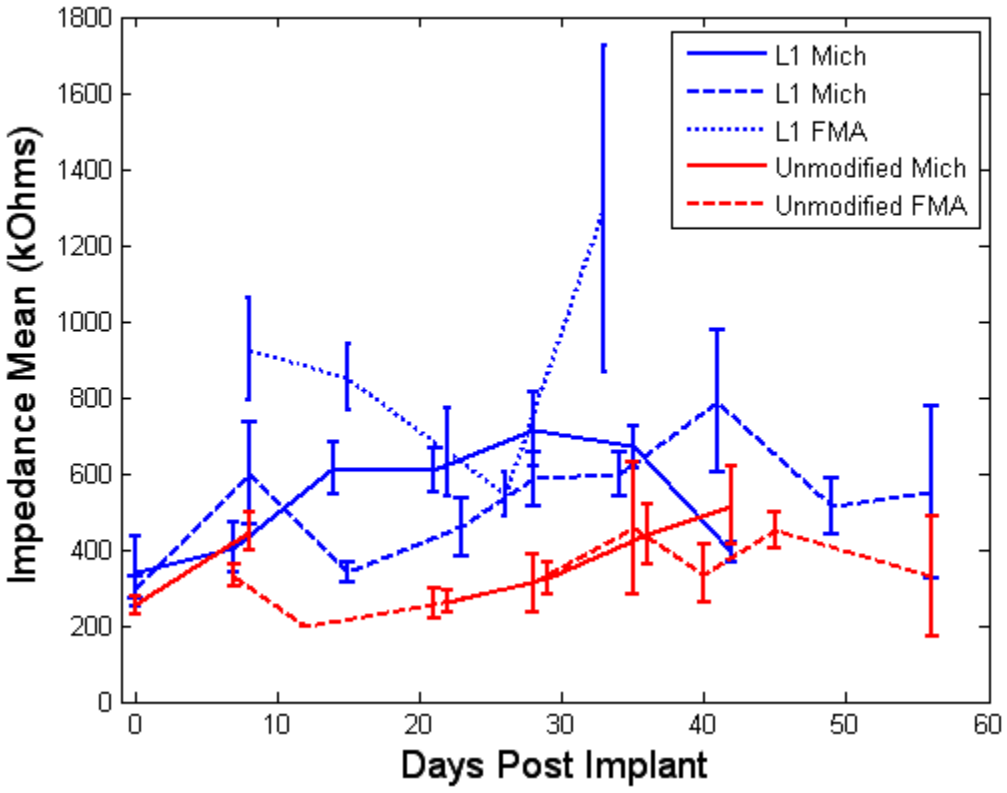

Figure 9. Mean Impedance over Time for 1kHz. Each probe is plotted individually. Certain probes did not provide a reliable signal for the entirety of the lifetime of the rat.

Figure 9 shows the average of the 1kHz impedance of valid channels for each experimental probe. A sweep of impedance measurements was taken at several different frequencies. These were then evaluated for consistency. A window of three points above and below the 1 kHz frequency was taken. A log-log transform was used, and linear regression was applied to this window of data. An R^2 statistic of at least 0.7 was required for the channel to be considered valid. If the reading passed R^2 test, then the fitted line was used to extrapolate the 1 kHz impedance. Due to equipment failure, Michigan control data could only be measured through week six.

The current data suggests that the L1 surface modification might in fact raise the impedance of surface enhanced electrodes slightly, although this may also be due to supporting components of the modification. However, most impedance values are still well within the acceptable range for good signal, and the sample size is still too small to suggest any definitive effect. The level of uncertainty in our data as evidenced by the poor recordings makes it impossible to draw any conclusions from the impedance data.

3.2 TIME COURSE OF SIGNAL DECAY

The raw quality of a signal often dictates the ability of a researcher to decode any useful information from it. Two major categories of data signal used for neural signal decoding are the high speed neural “snips”, and the slower speed LFP. Parameters reflective of each of these two types of signal were quantified.

Neural spikes are generally detected with an amplitude threshold. If the noise value is sufficiently high, it becomes completely impossible to detect any neural spiking event. It is desirable to maintain a low noise floor so that the maximum number of isolatable units may be collected.

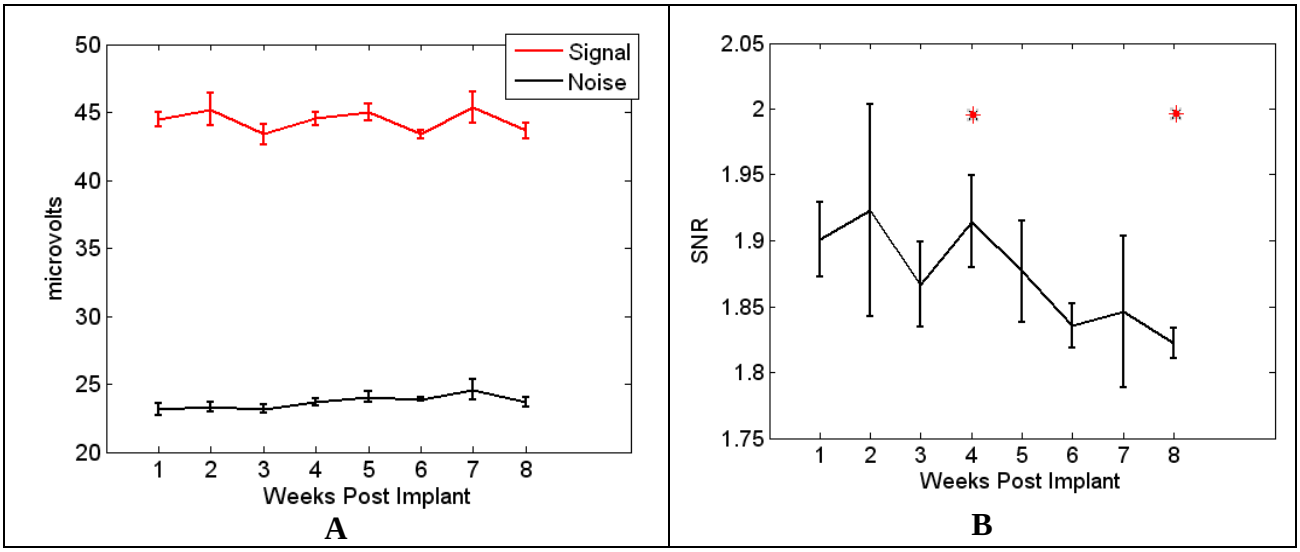

Figure 10: Signal to Noise of all Probes. (A) Comparison of Signal vs Noise at weekly time points. (B) Mean SNR over 8 weeks. A multiway ANOVA was applied to identify significant differences in the data over time. Because of the low samples size, $p = 0.075$ was used. Color pairs of * indicate pairs of data that were significantly different. A burst stimulation trial from the unmodified Michigan probes was used. n = 32.

Figure 10 shows the computation of signal to noise ratio over 8 weeks. Figure 10.A shows the typical levels of signal and noise over time. The RMS value of a 1 second segment of high pass filtered data was computed and averaged for each channel of each experimental group (n=32). The noise floor was characterized as 2x the RMS value of the high pass filtered neural data stream. [7] The peak to peak amplitude (PPA) of the signal was computed by collecting a population of waveforms, computing the mean waveform, and taking the maximum and minimum points of this trace. The high pass filtered noise tends to be fairly stable, while the majority of the loss of signal quality can be attributed to decreases in the peak to peak amplitude of the signal. Figure 10.B shows the average of the signal to noise ratio (SNR) of the two unmodified probes. We feel this represents a characterization of the expected time course of the decay of SNR. The observed time course of SNR makes sense in consideration of the two phases

of tissue reaction. Initially there is an improvement as the acute response returns to normal, and then the signal decays as chronic gliosis sets in.

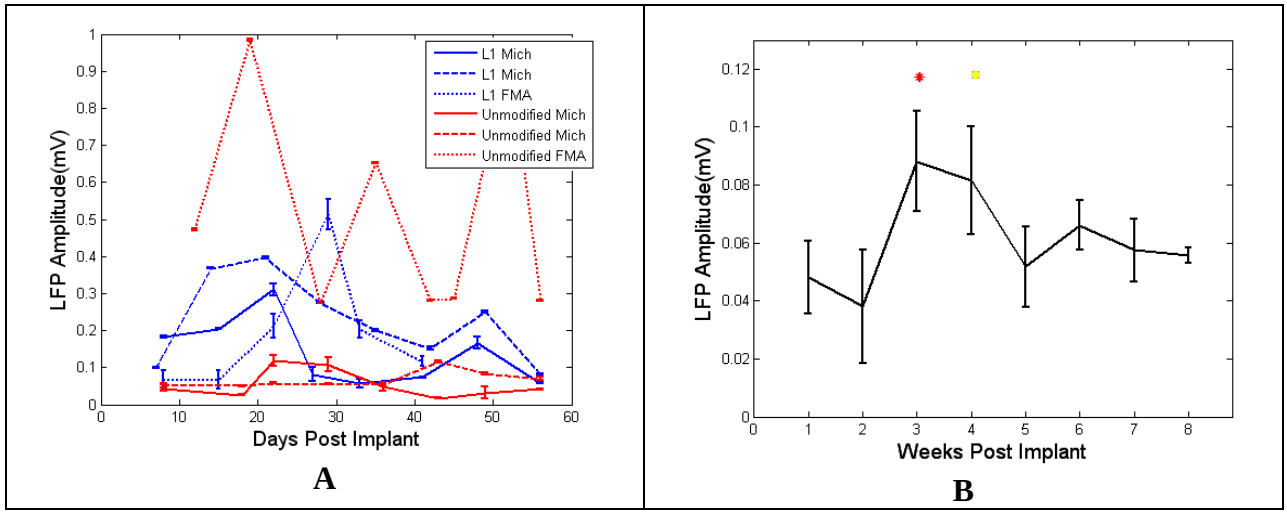

Figure 11: Local Field Potential Peak to Peak Amplitude over Time. (A) Average PPA of the LFP of a spontaneous trial per probe (B) Characteristic time course of LFP PPA over time. The two unmodified Michigan probes were considered to be representative of the tissue's most natural response, and were averaged for this plot. A multiway ANOVA was applied to identify significant differences in the data over time. Because of the low samples size, $p = 0.1$ was used. Week 3 (red *) is significantly different from all points except week 4 (yellows *). Week 4 (yellow star) is significantly different from all points except weeks 4 and 6. n = 32.

Figure 11.A shows each of the 6 probes included in the study plotted individually. LFP amplitude is calculated as the difference between the 5th quartile and the 95th quartile in a spontaneous trial. There is a significant amount of day-to-day variability in the control FMA. This is likely due to the lack of a faraday cage and the dynamics of awake recording. We attribute the decline in signal PPA to neuronal cell death and the expansion of the electrode track's kill zone. Figure 11.B shows the two unmodified Michigan electrodes averaged together.

There is a similar trend present as is shown in SNR in Figure 10.B. An initial increase in the PPA is seen in first few weeks, and then a slower decline over the remainder of the study.

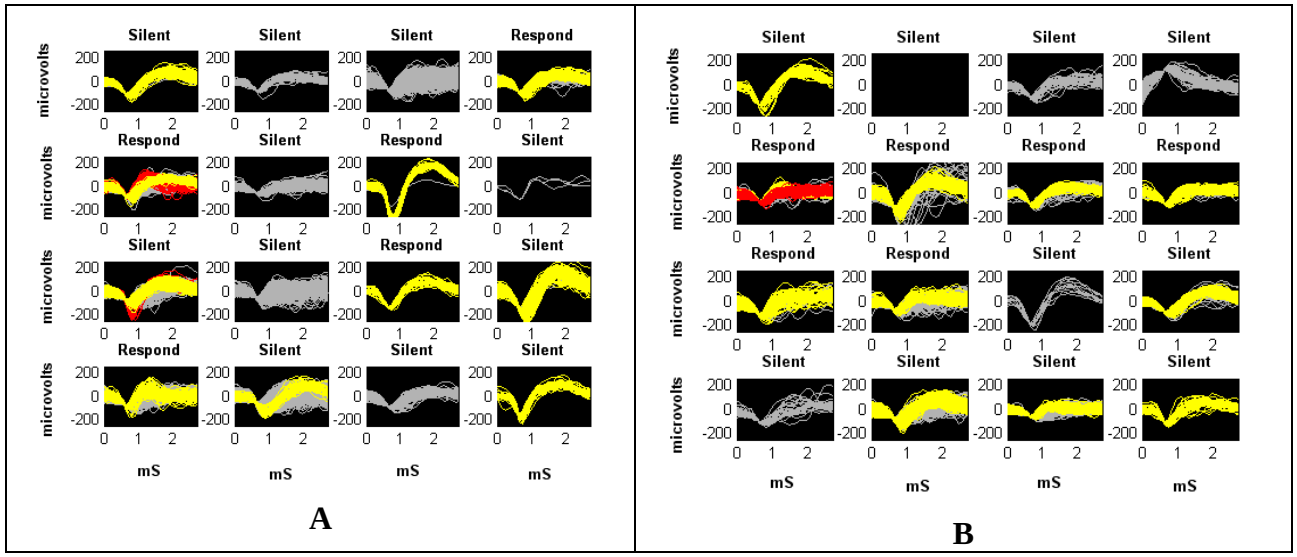

Figure 12: Waveforms of 16 channels on Two Days. Channels are labeled "Respond" if either single unit responds to the stimulus, and "Silent" if not. (A) day 40 (B) day 42.

Figure 12 provides an example of some of the original waveforms, and an illustration of the justification for offline thresholding. Depending on the SNR of any given recording, the window of successful spike detection can be only a few microvolts wide. The exact location of this window can change within the duration of one recording. If the threshold is too high, the system will miss a valid unit. If the threshold is too low, excessive noise will be introduced into the signal, which can hide the presence of a valid unit under snips of noise. This problem is further expressed when multiple units are present as the distinction between the two units is often dependent on a carefully set threshold. See Appendix B for a detailed description of the algorithm used for offline thresholding. The lack of day-to-day consistency due to the differences in the ways that thresholds are set at two different times can cause units to appear less stable than they really are.

The second FMA was analyzed with offline thresholding. This resulted in a much more reproducible signal. However, FMA 2 did not exhibit the same quality of neural waveforms as FMA 1. This may be attributable to the fact that recordings were conducted under anesthesia, or it may simply be caused by differences in the biological reactions. Further investigation is necessary.

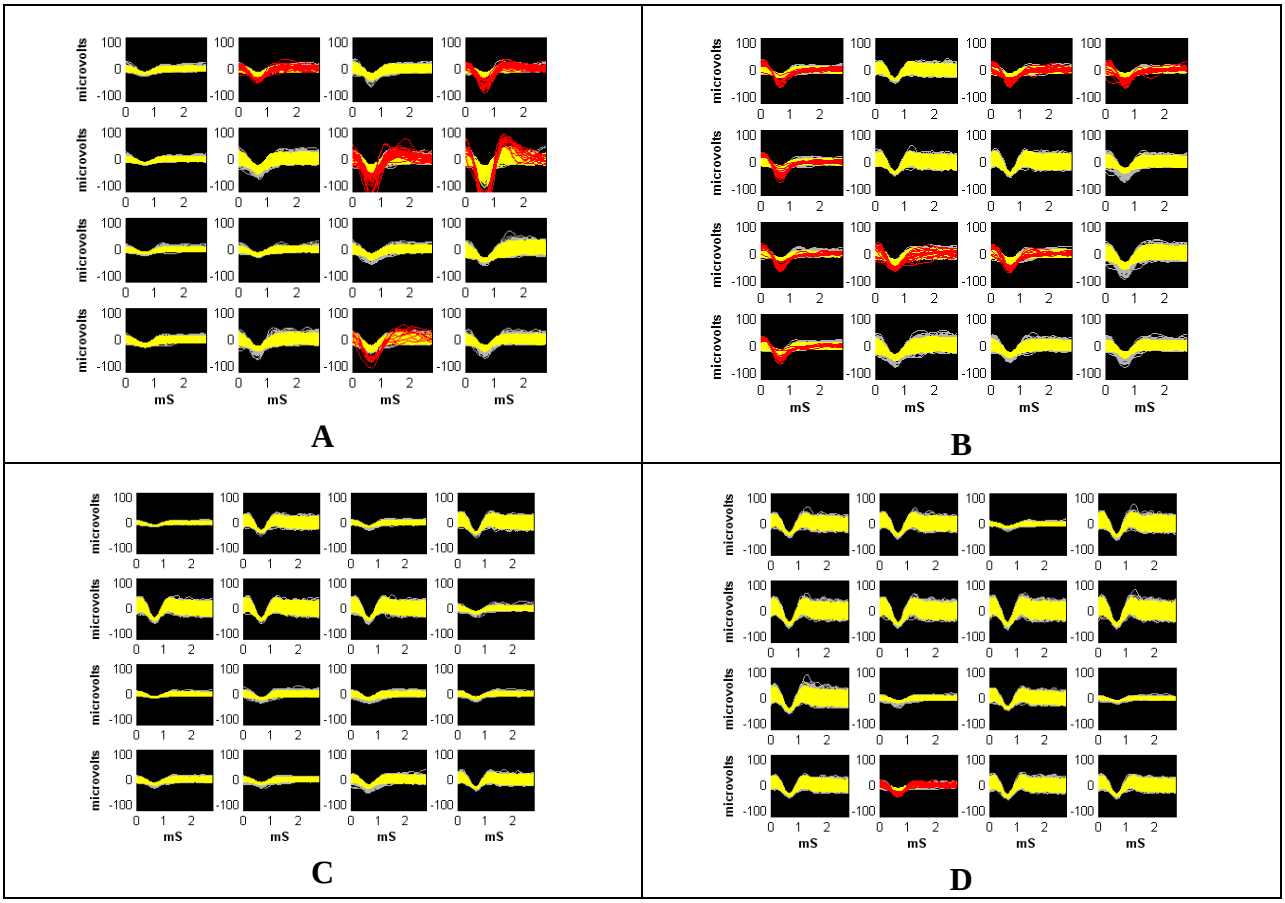

Figure 13: FMA 2 Example Units. (A) 3 weeks. (B) 4 weeks. (C) 5 weeks. (D) 6 weeks. Gray is the unsorted category, yellow is the base unit. Red is an isolatable single unit.

Figure 13 shows an example of the sorted waveforms found on all 16 channels of a simulation trial for 4 different time points. The offline snipped waveforms are more consistent

day to day, but the lower quality of this electrode makes it difficult to conclude how much the overall signal quality is improved.

3.3 COMPARISON OF SURFACE MODIFICATION

The same data used to characterize the typical parameters of chronic signal quality can be divided into experimental groups. Although n=2, certain trials show trends between the L1 probes and the unmodified probes.

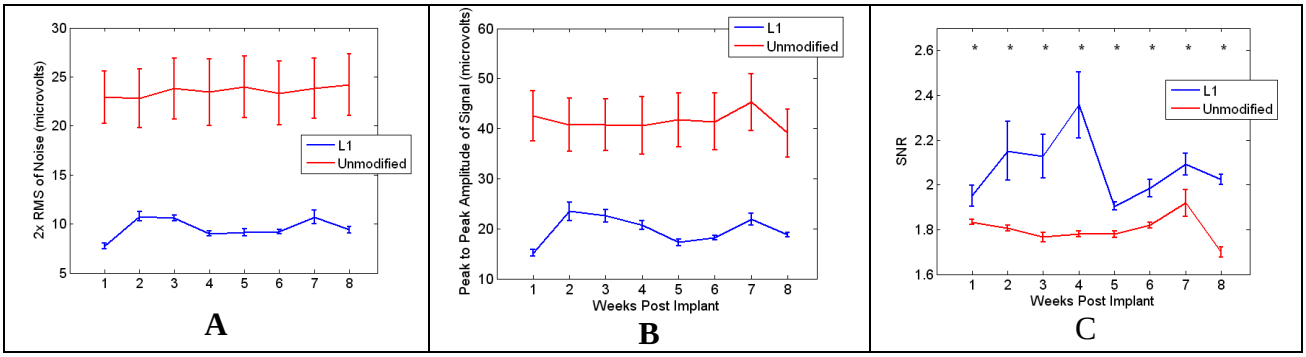

Figure 14: Signal and Noise over Time (Single Shot Stimulations). (A) 2x the RMS value of the noise floor of the signal. (B) Peak to peak amplitude of the mean waveform. (single shot stimulation trial, n = 32, SEM values plotted on the axis.) (C). Signal to noise ratio was computed by dividing the peak to peak amplitude of the snips by 2x the RMS value of the noise. A Student's t-test was used to compare the two coatings. The * indicates significant difference (p = 0.05) between the two categories on the SNR plot.

The SNR provides a better estimation of the quality of the electrode interface than any of the simpler parameters. Figure 14.C shows that the L1 modification has a higher SNR than the control. The higher SNR means that the snips are rising higher above the noise floor in the L1 modification, making the signal easier to detect.

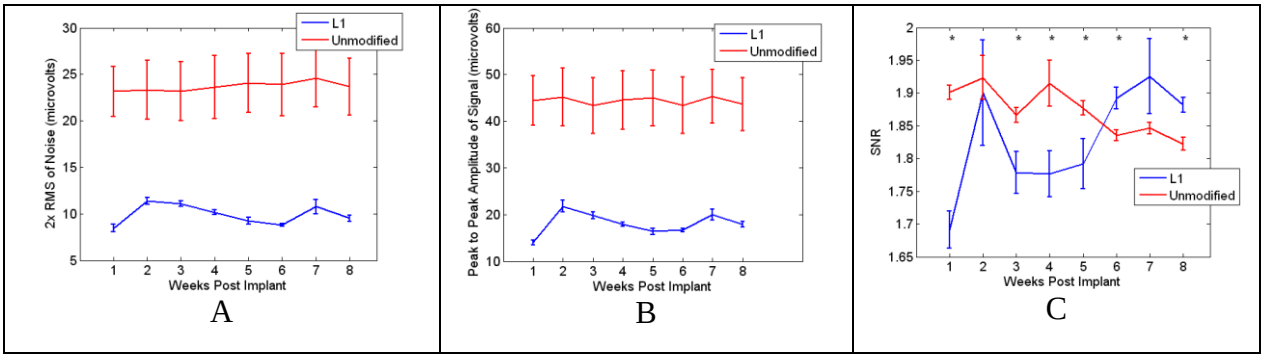

Figure 15: Signal and Noise over Time (Burst Shots Stimulations). Subplots are the same as Figure 14.

Figure 15 shows the same analysis as Figure 14, except that the data is collected from a burst stimulation trial. The unmodified trace is the previously shown characterization of SNR (Figure 10). In this trial the L1 coating does not show a consistent improvement over the unmodified probes. However, as will be shown later, the time course of the unmodified probe from this trial correlates better with other measures of signal quality. Figure 15 suggests that the effect of L1 on improved signal quality may be specific to certain types of signal.

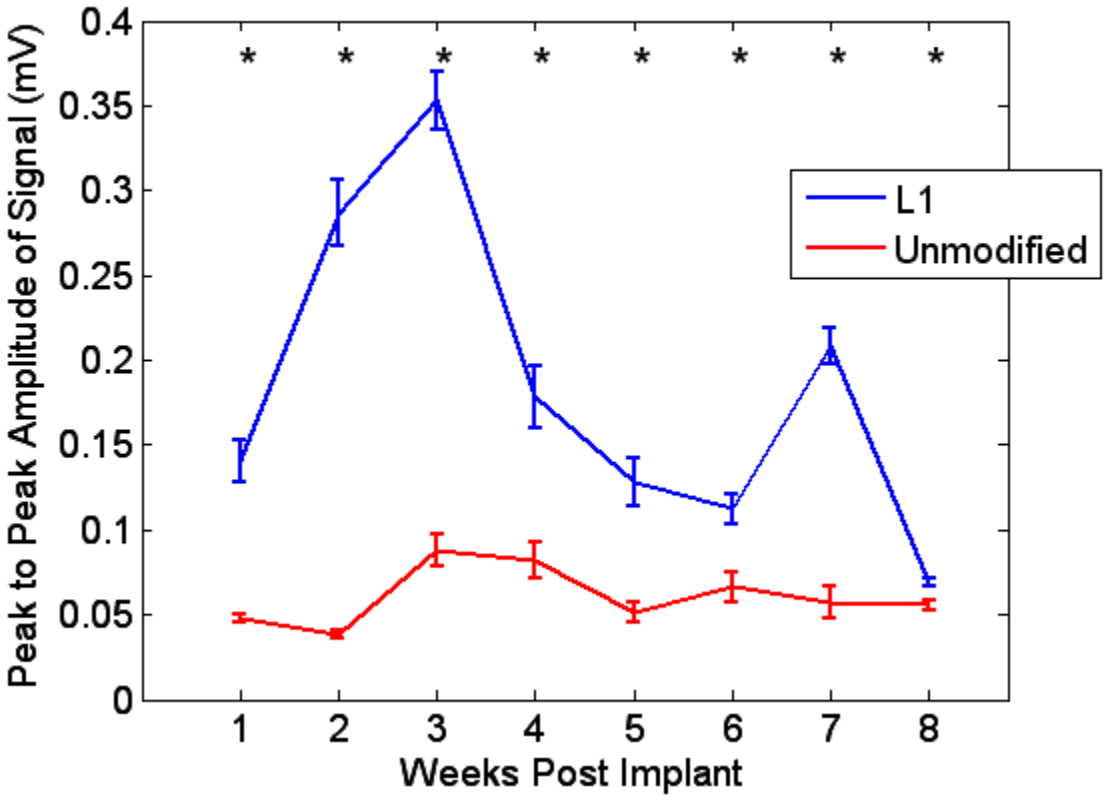

Figure 16: LFP Amplitude over Time. The difference between the 5% and 95% quartile of a segment of spontaneous activity for each channel was computed and averaged by experimental group. (n = 32) Only Michigan data is shown. All differences between the two categories are shown to be significant with a Student's t-test; $p < 0.05$.

A final measure of signal quality is the level of energy contained in the LFP data. [6, 7] Figure 16 shows a comparison of this data. This is somewhat of an arbitrary measurement since it is partially dependent on the depth of anesthesia, but it does provide a qualitative estimate of the health of the brain tissue local to the implant, and the strength of the signal reaching the electrode. The L1 probe modification shows significantly higher peak to peak amplitude than the spontaneous LFP, suggesting stronger neuronal presence in the area of the probe and a healthier implant site.

4.0 ISOLATED STIMULATION

A basic form of stimulation to the rat barrel cortex is to simply deflect the whiskers once. A single stimulation under this trial was delivered with a brief (100 ms) puff of air from a single jet at 20 psi. The puffs were delivered several seconds apart, and the LFP activity was allowed to return to baseline between stimulations. We assume the trials to be independent. Stimulation trials allow a different parameter of the implant to be measured. In addition to simply evaluating the raw components of the signal, the clarity and reliability of the information contained in the signal may also be evaluated. This basic form of stimulation was employed for all of the rats in the entire study.

Figure 17 provides an example of the combination of multiple trials to compute a characteristic response. As described in Chapter 3, the two major forms of signal that can be measured are the high speed "snips" and the lower speed LFP.

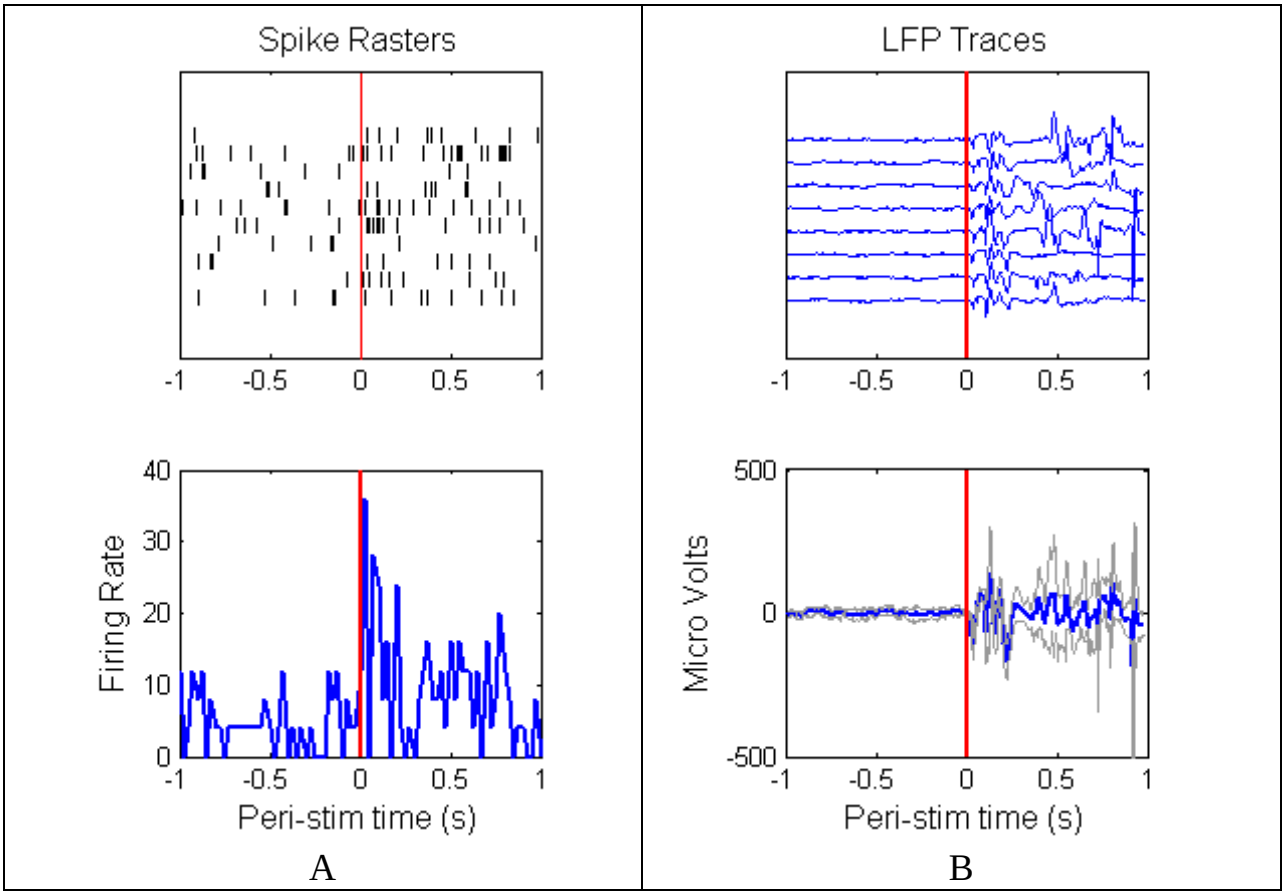

Figure 17: Overview of Single Stimulation. (A) The peri-stimulus histogram is developed by averaging together the raster plots from 10 different trials. (B) The LFP peri-stim trace is computed in a similar manner.

4.1 WAVEFORM ANALYSIS

A peri-stimulus histogram (PSTH) was constructed from the spike trains, extending one second before and after the stimulation. Data from approximately ten independent trials were averaged together to obtain a characteristic response.

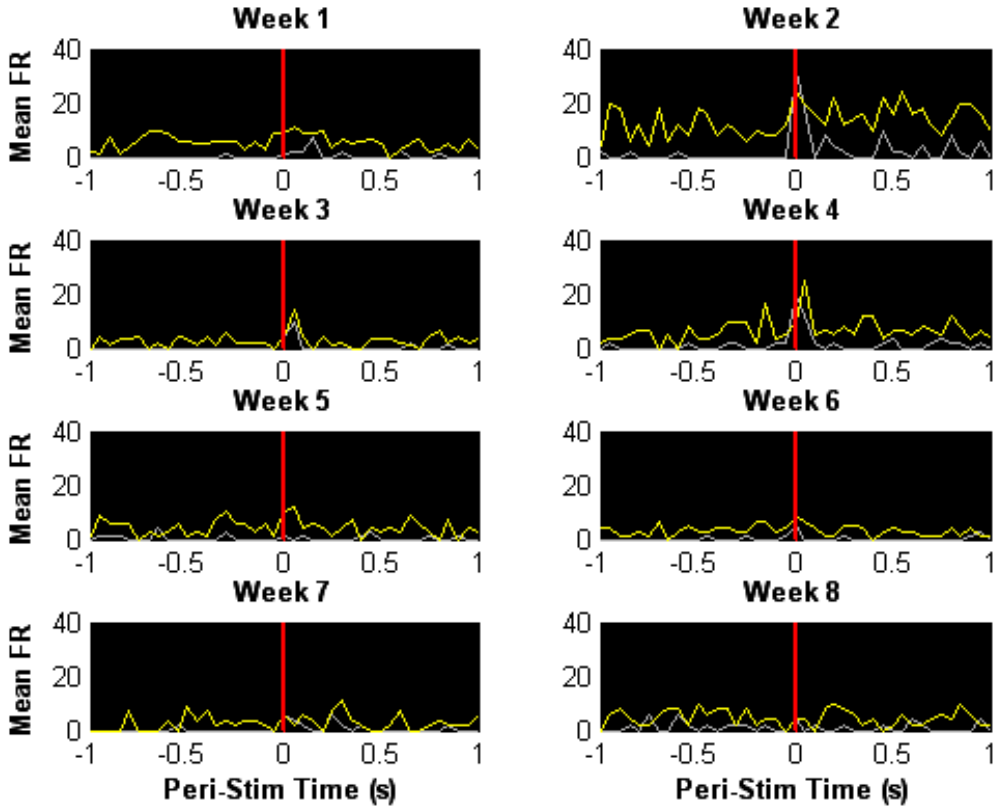

Figure 18: Example of PSTH Over Time. Approximately 10 stimulations were averaged together to develop a characteristic response. Firing rate was computed by counting the average number of spikes occurring in a histogram bin and dividing by the width of the bin. Bins 50 ms wid were used. Yellow shows the PSTH of the primary waveform. Grey shows the PSTH of the unsorted category.

Figure 18 shows an example of the peri-stimulus histogram of a single channel over 8 weeks. Offline thresholding improves the detection of evoked response by ensuring that enough spikes can be collected to compute a baseline pre-stimulus firing rate.

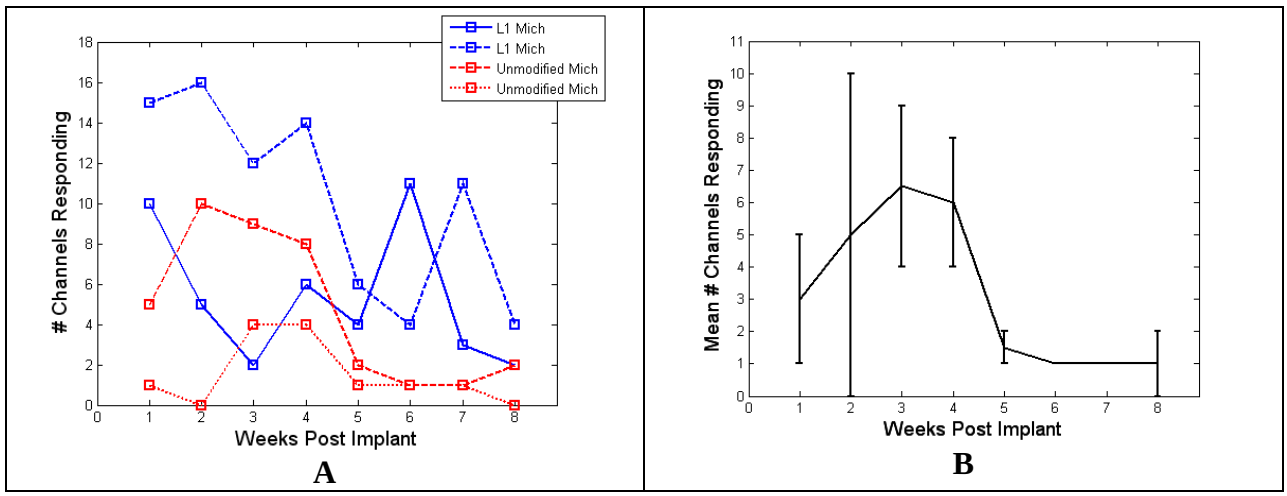

Figure 19: Number of Channels Responding Over Time. (A) Number of channels responding on each probe over 8 weeks. (B) The two unmodified probes averaged together. n = 2.

One common metric of determining the quality of an implant is tracking the number of channels that respond to a given stimulation. Firing rate was computed with a peri-stimulus histogram using 50 ms bins. In order for a channel to be considered to be responding, the mean firing rate of the sorted waveform, computed from multiple trials (Figure 17), must show a significant increase in firing rate within 250 ms immediately following the stimulation.. This was quantified with a one-tail student's t-test (p = 0.05) comparing a 500 ms window before the stimulation with 250 ms after it.

4.2 LFP ANALYSIS

The LFP responds more slowly and persists longer than the waveform response. As Figure 20 illustrates, the LFP responds out to 8 weeks with decreasing response amplitude.

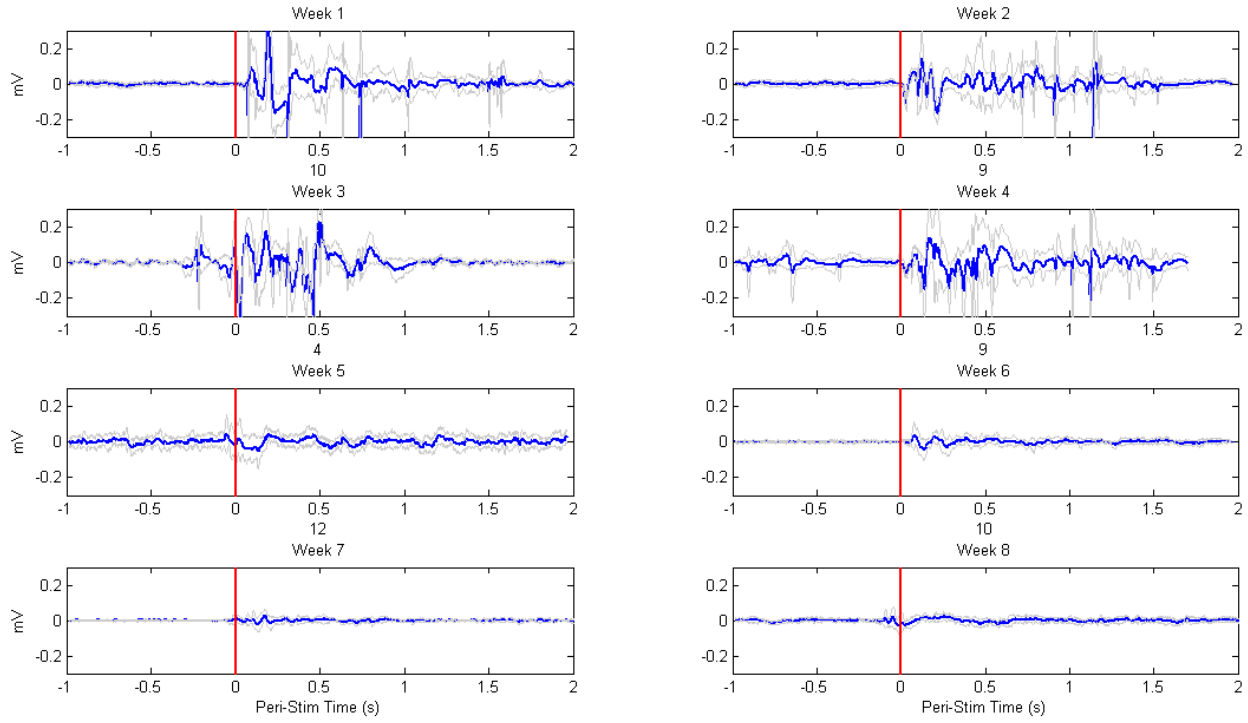

Figure 20: Example of LFP Peri-Stimulus Traces Over Time. Gray lines represent one standard deviation above and below the mean. Multiple stimulations were averaged together as in Figure 17.

Figure 20 shows an example of averaged LFP traces with a single shot stimulation. Trials were removed if a spontaneous burst occurred near the start of the stimulus. Tests were applied to this trace to quantify the number of channels responding to the simulation for each probe over time.

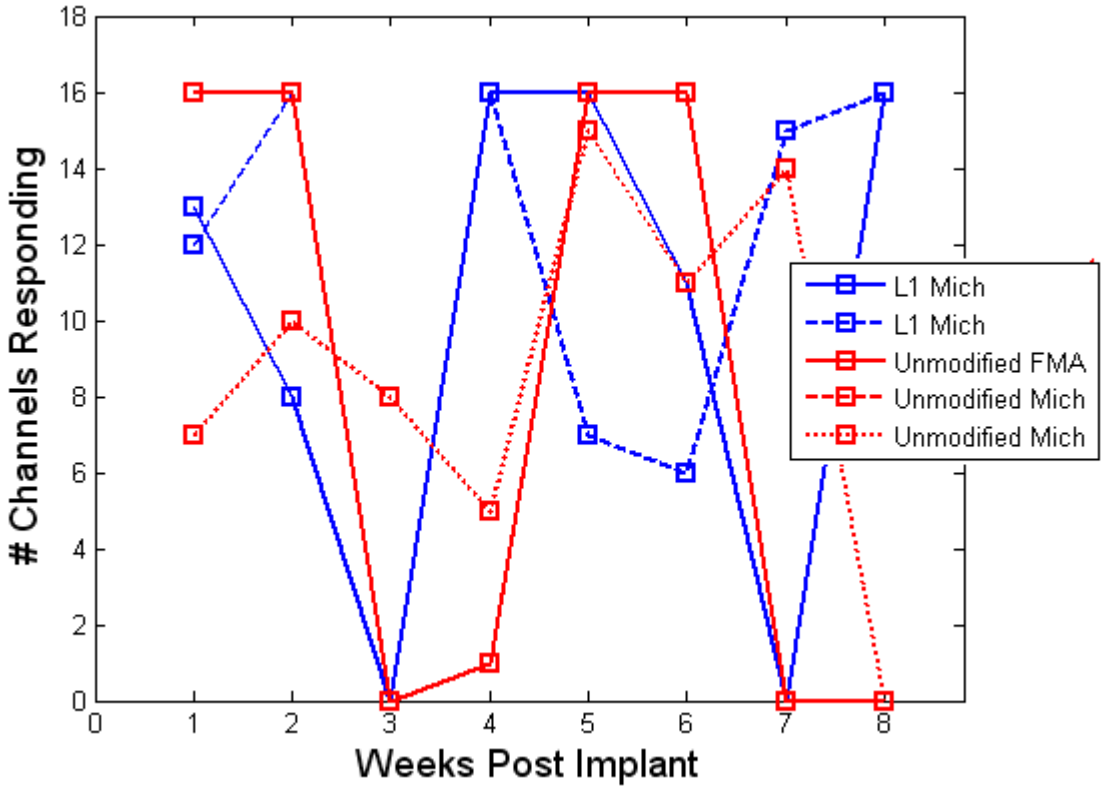

Figure 21: Number of Channels Responding with LFP over Time (Single Shot Stimulation). Each probe is plotted individually.

Figure 21 was developed by considering a window of 200 ms following a stimulation. The RMS value of this "post-stim" time was compared with the RMS of a one second window prior to the stimulation. If there was at least a twofold increase, the channel was classified as responding. The inconsistency of this plot suggests that significant refinements to the experiment are still necessary. An "all or nothing" trend is apparent from week three onwards. The continued response of the L1 probe at 8 weeks may suggest that L1 promotes a closer presence of neuronal tissue to the probe in a chronic implant.

5.0 SEQUENTIAL STIMULATION

A single stimulation is the simplest type of stimulation and provides the most basic form of input to a system. Much information about the quality of the tissue interface of a microelectrode can be determined from simple signal parameters. However, a functional neural prosthetic should be able to decode a variety of different information and the quality of a surface enhancement's ability to improve signal quality should be evaluated under a variety of different stimulation conditions. Furthermore, successive stimulation is in many ways a better representation of the natural stimulation that a rat receives in his native environment. The technique of sequential stimulation with the air jets was developed after FMA 1, and applied to all rats from there on.

5.1 WAVEFORM RESPONSE

At a neural level the single shot stimuli were designed so that each air puff would be an isolated event. The neural activity was allowed to fall to baseline between stimulations, and efforts were made to avoid overlapping with a spontaneous burst. In order to increase the complexity of the recording paradigm, successive stimulations were delivered close enough together that the individual shots combined into a longer stimulation. Previous research has shown that even stimuli as subtle as different surface textures selectively activate the barrel cortex. [50] We

hypothesized that stimulating at different frequencies would also selectively activate the barrel cortex and that responses would be characterized by spatial location and stimulation frequency, and that the amplitude and consistency of these responses would decay as the tissue reaction increased. Each stimulation burst was delivered for approximately 5 seconds, and at least 7 bursts per day were taken. In all bursts except the highest frequency trial, the duration that the solenoid valves were open (100 ms) was consistent, and the interval between opening the valves was adjusted to create a frequency specific stimulation. Due to the low level of anesthesia during the experiment, spontaneous activity was often present, so trials where a spontaneous burst coincided with the onset of stimulation were removed in order to simplify the detection of the response.

In this more complicated stimulation paradigm several common response patterns arose. One such pattern (termed "Adapting") appeared to respond to changes in stimulation. In this pattern, the cortex showed a response immediately at the onset of stimulation. A second pattern, (termed "Non-Adapting") was used to classify trials where the cortex responded for the entire stimulation. In order to be considered proportional, the trial had to show an increase in firing rate for at least 50% of the time the stimulation was applied. In the final category (termed "Facilitating") the strength of the response appeared to build slowly over the time that the stimulation was applied. If an individual recording channel exhibited any of these three patterns of response, it was classified as responding. Otherwise the channel was classified as not responding.

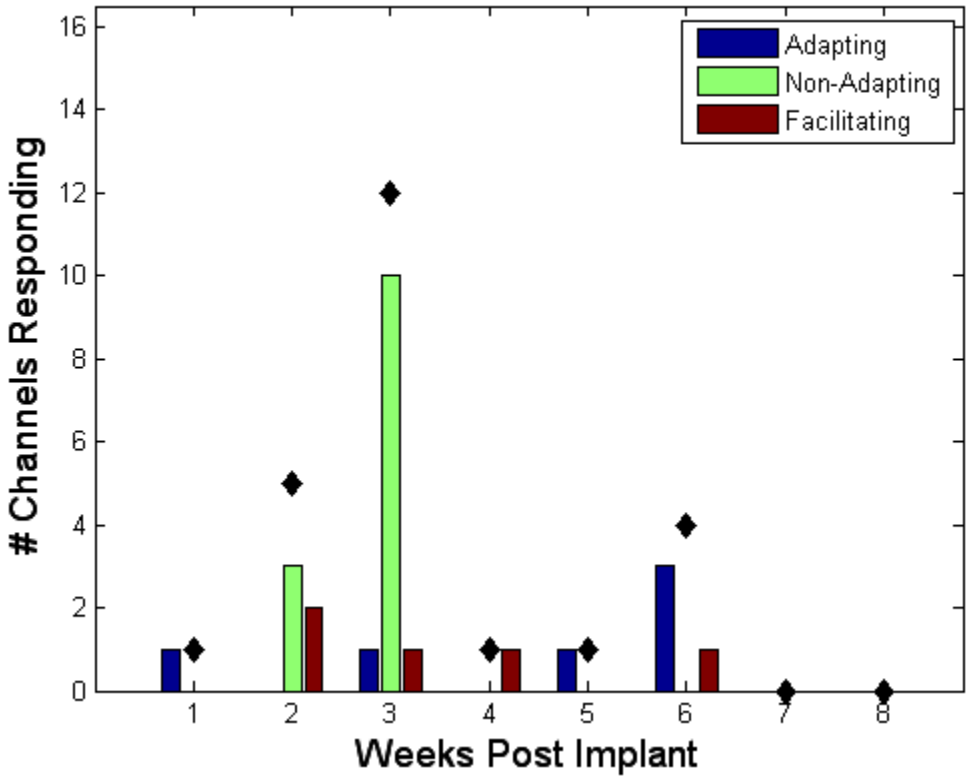

Figure 22: FMA 2 Waveform Response to 5 Hz Stimulation. Black diamonds indicate the total number of snips responding.

Figure 22 summarizes the results from FMA 2, the first rat in the study to be used with the burst stimulation. After completing this rat and determining that it was possible to decode responses from a burst of air puffs, it was decided to vary the frequency above and below the original 5 Hz frequency in order to increase the breadth of the study. 2 Hz was used as the low frequency stimulation for all rats except one (L1), which used 4 Hz for part of the study. 8 Hz was used as the high frequency stimulation for all rats except one (L1) which used 6 Hz as the high frequency stimulation.

The responses were characterized by comparing the time course of the firing rate post stimulation against the firing rate of two seconds prior to the onset of the stimulation using a one-tail student's t-test. Post-stimulus windows of progressively increasing length were used. If the trial showed a significant increase in firing rate when considering only the first 200 ms following the onset of stimulation, but did not show significance in any other windows up to 1.8 second, it was classified as adapting. If at least half of the windows used showed a significant response, the trial was classified as non-adapting. If a trial could be found that showed a significant increase, but did not fit one of the previous categories, it was classified as facilitating. The firing rates were computed using a peri-stimulus-histogram with 50 ms bins, and the post-stim window was increased in increments of 200 ms. Because this is a novel paradigm, a *p* value of 0.01 rather than 0.05 was used as the threshold for significance in order to increase the confidence in the detection.

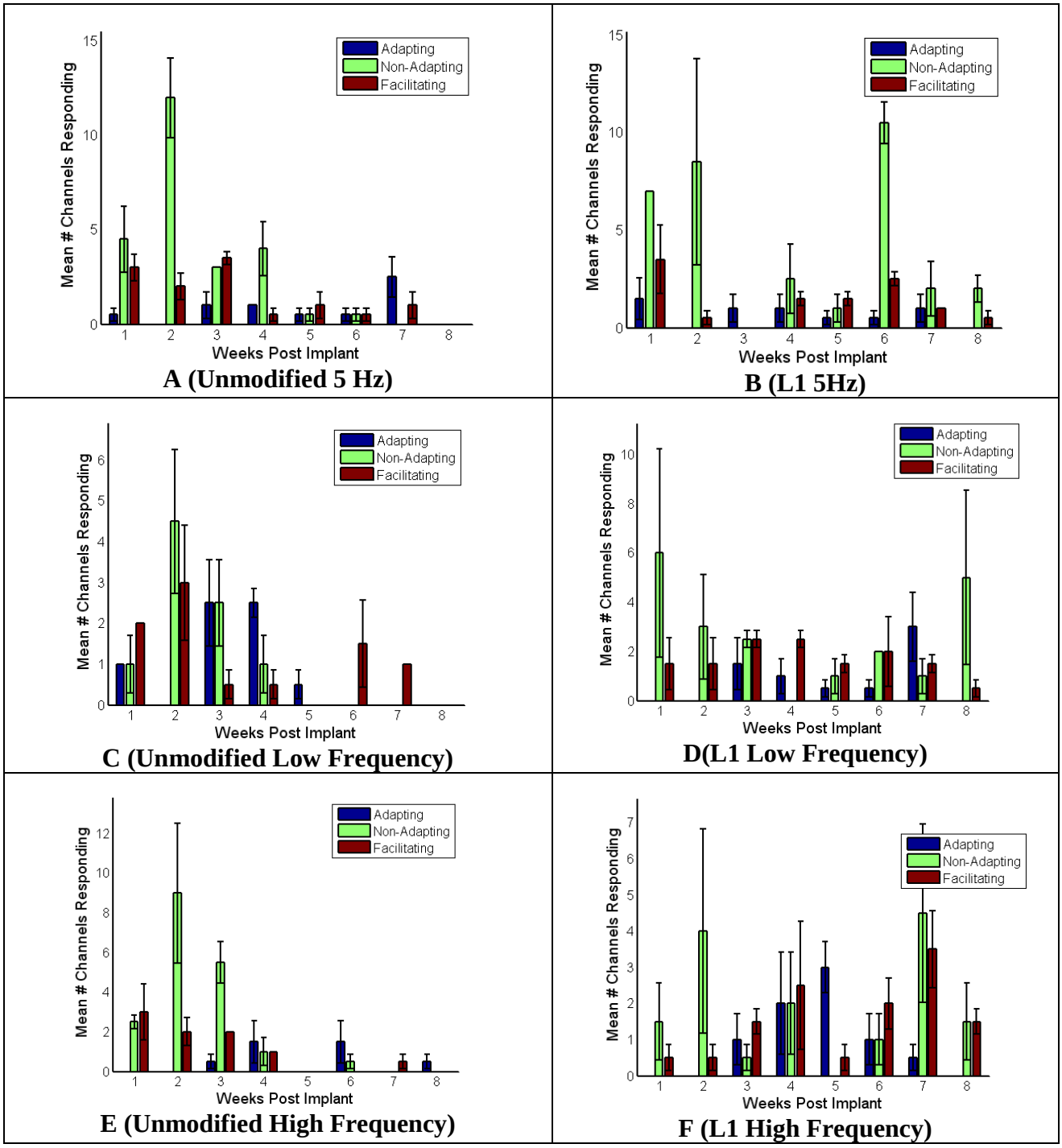

Figure 23: Sorted Waveform Responses to Frequency Stimulation (Michigan Probes). Counts of each different type of responses for each stimulation frequency are plotted. Unmodified (A, C E) L1 Modification (B,D,F) Data is not available for weeks 1 and 2 for high and low frequency in one L1 rat. Otherwise n=2 for each time point.

Figure 26.A-26.B shows the responses of the 5 Hz stimulus over time and by experimental group for the Michigan probes. The 5 Hz trial showed a strong presence of the non-adapting response early in time, and except for week 5 of the L1 probe, a more balanced distribution of the different categories later in time.

In addition to the 5 Hz stimulus, a stimulus was delivered at a lower frequency and at a higher frequency. Typically 2 Hz was used as the low frequency and 8 Hz was used as the high frequency. These were selected partially because of the limits of the solenoid valve system. The low frequency stimulus was intended to allow more time for the cortex to recover, and perform similarly to the single shot stimulus. Figure 26.C-26.D shows the results of the 2 Hz frequency stimulation. With this trial, the loss of the ability to record at the later time points in the unmodified probe is more pronounced. Also of note is the increased presence of the facilitated responses late in time, possibility suggesting some changes in the tissue as the chronic tissue reaction advances. Figure 26.E-26.F shows the responses for the 8 Hz stimulation. In this trial it was necessary to shorten the puff duration to 62.5 ms. Although it has been shown that the rat barrel cortex can discriminate stimulation frequencies in excess of 20 Hz, the 8 Hz frequency began to reach the limits of the air jet puffer system, as the jets of air begin to blend together to create a turbulent wind. [51] Were the frequency to be pushed sufficiently high, the color of the noise would become increasingly occluded as the shorter puffs mixed on the way to the rat. This trial is the highest level of energy applied to the rat.

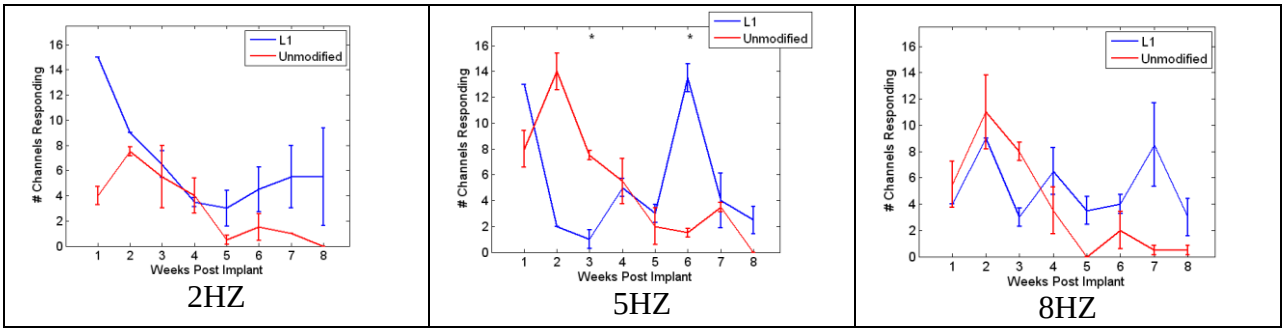

Figure 24: Mean Number of Channels Responding with Waveforms at Different Frequencies. Total count of channels responding for each day. All 3 types of responses are counted, and the experimental groups were averaged together. The * indicates statistical significance of $p < 0.05$ (Student's t-test). n=2

Figure 24 shows a comparison of the strength of response for each stimulation frequency as well as the consistency. The 2 Hz stimulation is closer to the single shot stimulus and may provide a simpler level of input to the cortex. The 8 Hz stimulation moves the whiskers at the highest frequency contains the highest energy level in the input signal. In all stimulation frequencies the control probes show an increase in the number of responding channels between weeks 1 and 2, and then a decrease in the number of channels responding. We hypothesize this to be related to the biological transfer between the cessation of inflammation and the onset of chronic gliosis.

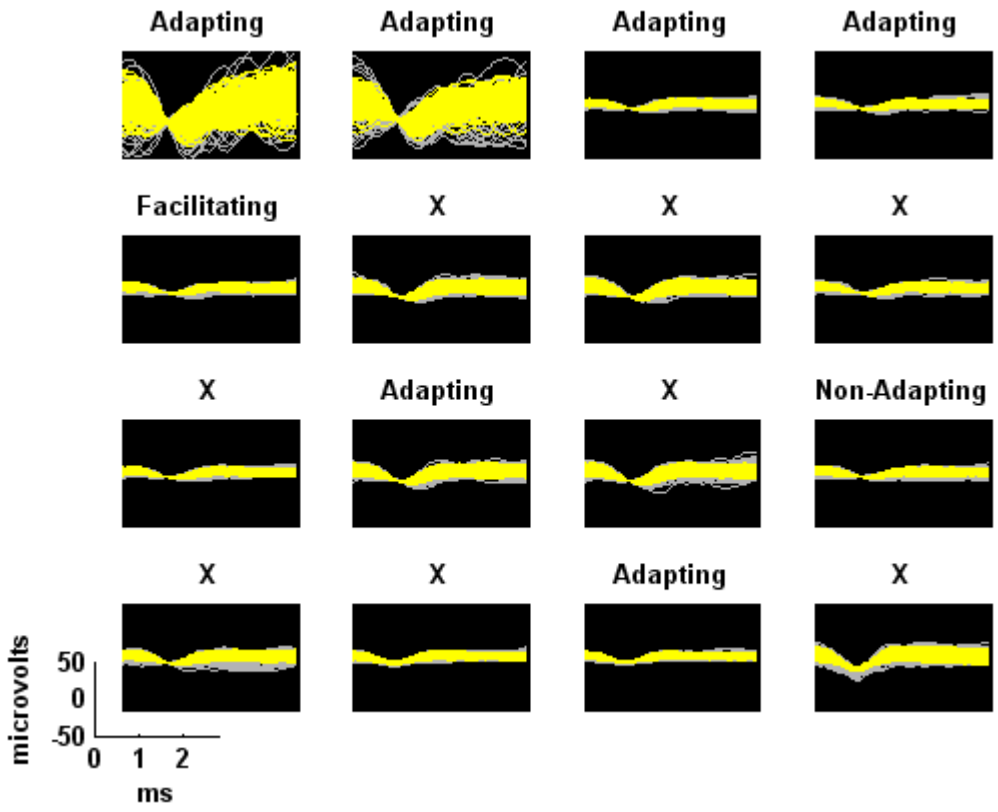

Figure 25: Example of Waveforms Corresponding to Sorted Responses. The waveforms used to generate and classify the burst peri-stimulus historgram (PSTH) are plotted. Yellow is the multi unit category, and grey is the unsorted category. Outliers were removed. Waveforms were isolated with offline thresholding. (5Hz stimulation unmodified Michigan rat 1, week 4)

Figure 25 shows the waveforms that correspond to different types of responses. Some correlation between the quality of the waveform and the ability of the system to detect a response is expected. However, note that although stronger waveforms often result in a strong form of response, this cannot be established as a consistent principle.

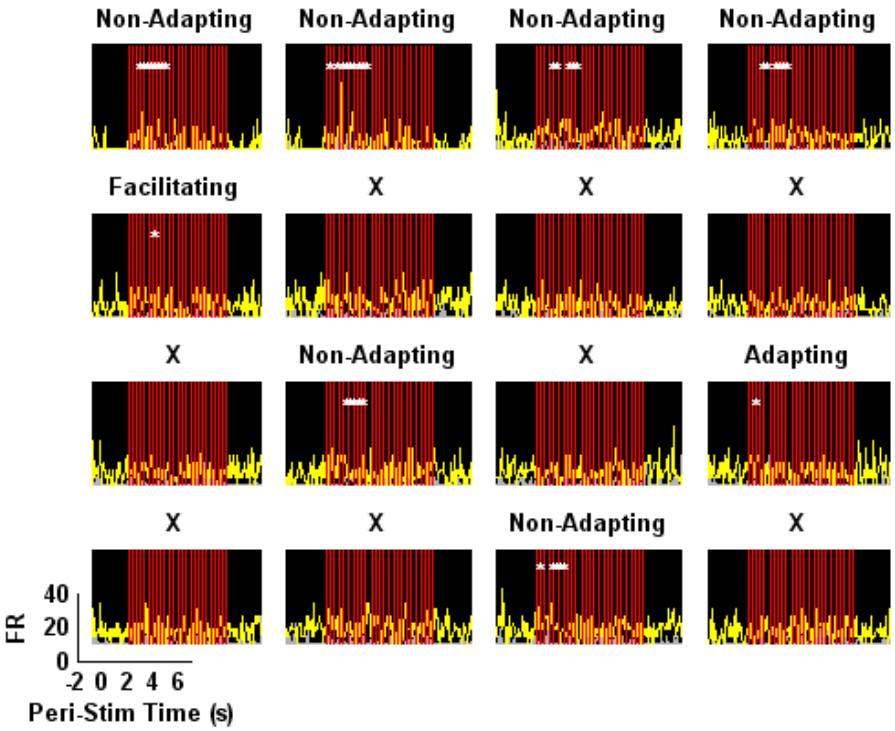

Figure 26. Example of PSTH Corresponding to Sorted Response. The firing rate is computed by averaging the spikes across several trials and dividing by the bin width of the histogram. X indicates no response. 50 ms bins were used. White * indicates the front end of a window containing a significant response. All windows start at time = 0.

Figure 26 shows the PSTH of the waveforms displayed in Figure 25 as well as the category into which they were sorted. Appendix D contains further examples.

5.2 LOCAL FIELD POTENTIAL RESPONSE

The LFP represents a summated response of an entire region of the cortex. The response is slower than the waveform response, and must be analyzed as a continuous signal, rather than a

digital signal. Figure 27 shows the categorization of different LFP responses to 5 Hz stimulation for FMA 2. The LFP was analyzed slightly differently than the waveform data. The data stream was divided into 200 ms segments, and the RMS value of each was computed. If more than 50 % of the windows showed at least a twofold increase in RMS from the pre stimulus RMS value, the trial was classified as non-adapting. If there was a twofold increase within the first second, the trial was classified as adapting. If there was a twofold increase at any other point while the stimulation was on, the trial was classified as facilitating.

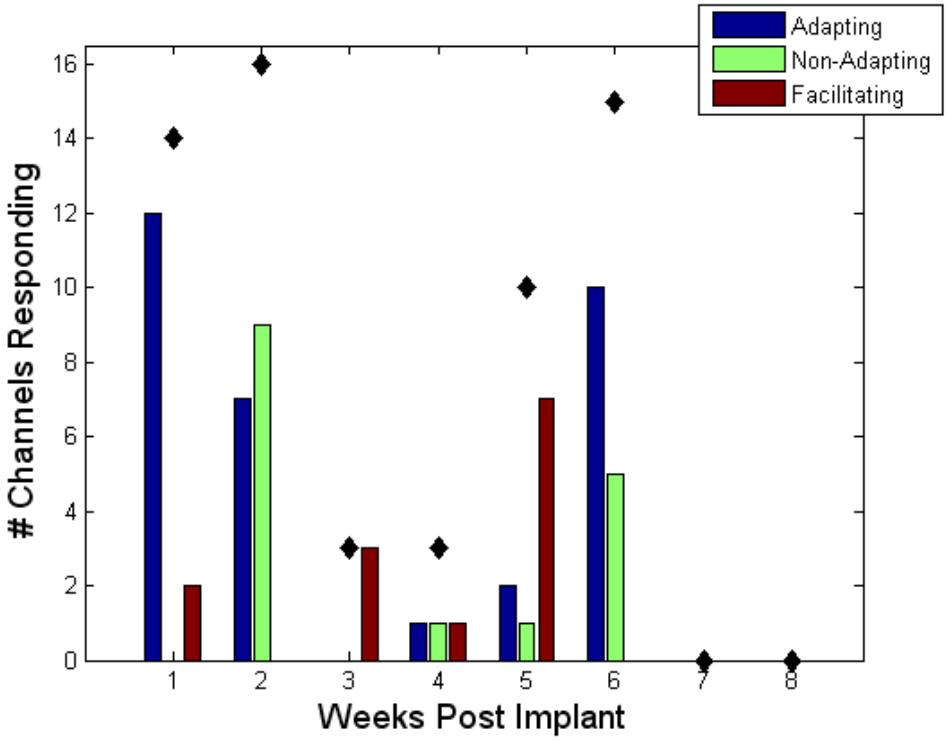

Figure 27: FMA 2 Sorted Response to Sequential Stimulation (5Hz) in the LFP Domain.

Figure 27 shows the response of FMA 2 L1. This was the second probe used in the study, and the first one to be used with V.2 of the recording system. This trial is more complicated, and the response tends to be more variable than the single shot stimulation. However, there is more

information contained in the signal, providing for the potential of a more detailed analysis paradigm.

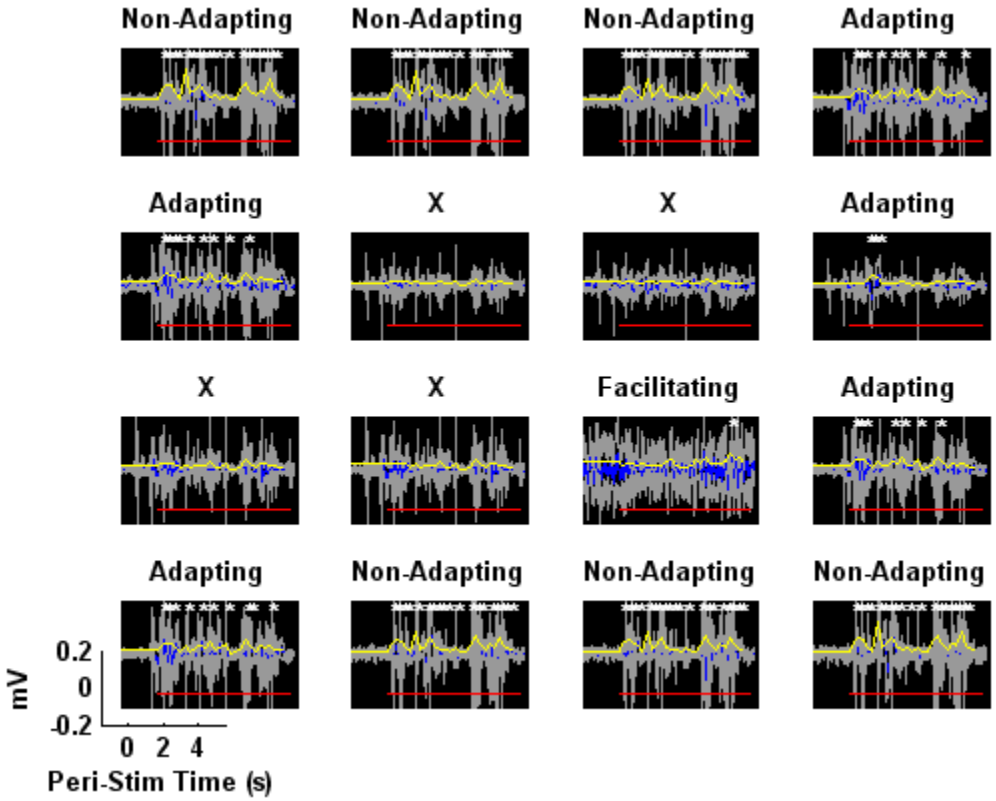

Figure 28. Example of LFP Sorted Responses. Blue is the mean of the signal, and grey is the standard deviation. The red line indicates the presence of the stimulus. White * indicates an RMS increase of at least 2x from the pre-stim value. (5Hz stimulation control rat 1, 1 weeks)

Figure 28 provides an example of the classification of the types of per-stim traces. This figure illustrates the differences in races for the three categories, as well as the difficulty in decoding from LFP. Appendix D contains several more examples.

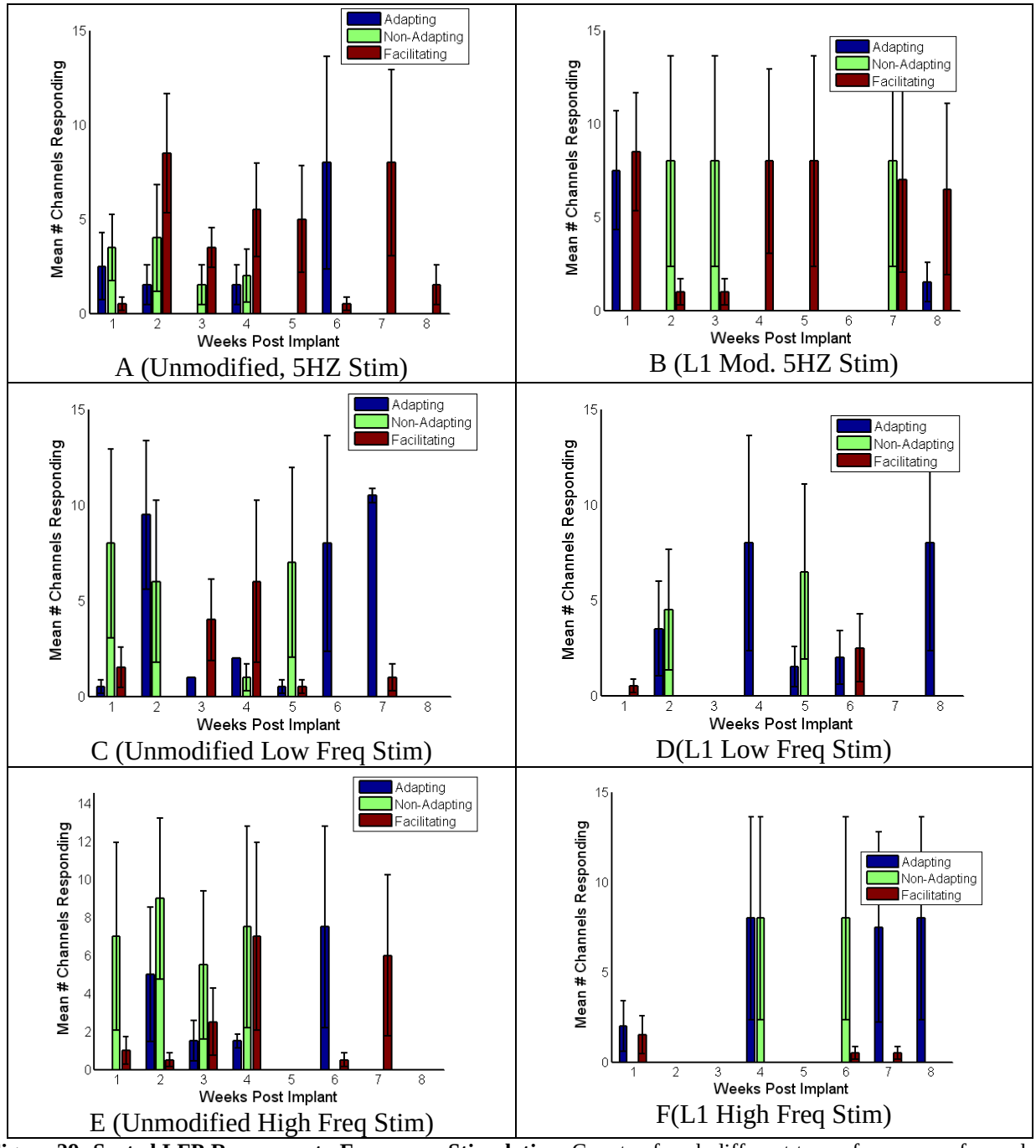

Figure 29: Sorted LFP Responses to Frequency Stimulation. Counts of each different type of responses for each stimulation frequency are plotted. Unmodified (A, C E) L1 Modification (B,D,F) Data is not available for weeks 1 and 2 for high and low frequency in one L1 rat. Otherwise n=2 for each time point.

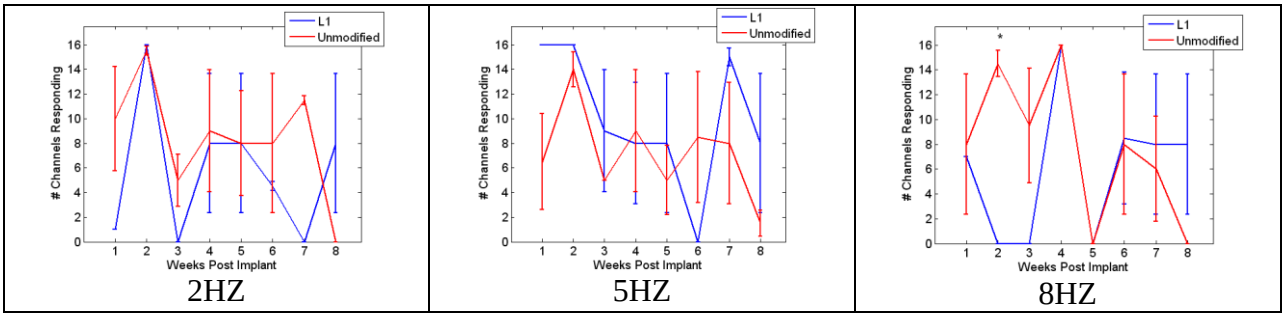

Figure 30: Mean Channels Responding in LFP at Different Frequencies. Total count of channels responding for each day is plotted All three types of responses are counted, and the experimental groups are averaged together. n = 2. The * indicates significant difference between the two categories (p = 0.05) n = 2.

The LFP data exhibits a high degree of variability in the nature of the response to stimulus. After the first two weeks, it is difficult to reliably record signal from any rat, regardless of the surface modification. The spontaneous bursting of the cortex at low anesthesia is a confounding factor in this experiment. Figure 30 shows an example of the classification of different responses. In most case the standard deviation is quite high, suggesting that the cortex does not respond consistently.

6.0 DISCUSSION AND CONCLUSIONS

6.1 IMPEDANCE MEASURMENT

The impedance data was impacted by high noise levels and low repeatability. Ideally it is possible to use the entire frequency spectrum to perform equivalent circuit modeling which can be reflective of cellular interactions. [6] This is a well established method of tissue analysis. The Cole-Cole equation is a common equation to represent the complex impedance of biological tissue. [28, 30]

$$Z = R + \left(R_0 - R_\infty\right) \Big/ \left[1 + \left(j\omega/\omega_0\right)^\alpha\right]$$

In this equation, R_∞ is the high frequency intercept and R_0 is the low frequency intercept on the complex plot. This equation can correspond to a few different RC circuit models, the details of which can be tuned to the needs of the individual study. [29] One study suggested a circuit model with different compartments for the electrode component, the tissue encapsulation component, and the cellular compartment. Such a circuit has a distinguishable frequency response. A full spectrum of complex impedance data would permit fitting similar models. Williams et al, 2007 showed that the real and complex components of this circuit are impacted in specific ways as the brain tissue changes. [6]

However, we struggled to reliably report the impedance of a single frequency point. The 0.7 threshold of the R^2 statistic was selected because it was the highest value that allowed about half the data to be classified as valid in the log-transformed linear regression. The weakness of this value as a fitting statistic is reflective of the low quality of the data. For this reason no conclusion can be drawn from the impedance measurements. The non-significant trends that are apparent are that impedance tends to be relatively stable for at least 8 weeks in our experimental design, and that L1-coated probes may have a tendency towards slightly higher impedances.

Several improvements can be made in the method of measuring the impedances. Most of these are related to improving the quality of the wiring between the probe and the device used to measure impedance. Another technique would be to use a site on the probe (such as the reference or the ground) as the reference for the impedance. This would eliminate the inconsistency in connecting to the skull screw and remove the potential for that connection to be interrupted by blood or debris. The trade off is that the new reference site would be significantly smaller, and impedances measurements taken would reflect the tissue reaction local to this site as well as to the probe recording sites. Finally, the majority of our recordings were taken using a sin wave with an RMS voltage of 5 mV. Increasing this value would provide a larger signal which would be more robust in the presence of noise.

6.2 LFP PROBLEMS

Isoflurane is known to reduce the amplitude and increase the latency of evoked potentials in rats. [49] It was decided during the planning phase of the experiment that this problem would be

acceptable since the goal of the experiment was to compare the coating and the effect would be consistent across the experimental groups. Isoflurane is metabolized quickly, and can be easily administered without risking accidental damage to the sensitive implant. However it was found that the exact depth of anesthetic was difficult to maintain and we lacked a good method of measuring anesthetic depth other than the degree of evoked response. This is a likely source of the inconsistencies apparent in the LFP data. Future experiments will control both the concentration of anesthetic that is administered to the rat, as well as the duration of the anesthetic. The experiments reported here controlled only the concentration of the drug.

The recording system was designed to be able to take advantage of the rat's ability to precisely differentiate spatial stimuli. However, the three different locations (Figure 8) of the air jets tended to produce very similar responses. This was likely due to the anesthetic and the problems with the Michigan reference. Future studies may be able to make better use of spatially patterned stimulations.

6.3 EVOKED SIGNAL CORRELATIONS

The signal shot stimulation is an effective method of signal quality evaluation. FMA 1 suggests that it is possible to discriminate between different anatomical locations on the rats whiskers if good waveforms are available. Unfortunately most of the data that was collected with Version 2 of the puffer apparatus also used Michigan probes, and quality waveforms were not available. However, the design shows promise for future studies.

The burst data contains a wide variety of different types of responses. The adapting and non-adapting categories are the strongest responses. Adapting responses show a swift response to the stimulation which then declines as the stimulus continues. Often these trials would also burst at the offset of stimulation, responding to the change in condition, however, due to the way trials were delivered in sequence, it was not feasible to analyze this post-stim burst. This type of response occurs as the inhibitory interneurons suppress the activity in the spiny stellate excitatory cells. The facilitating category is the weakest response type. We believe that this category is a non-native response to the stimulation, and may be related to the damage caused by the implantation and the scaring response. As the chronic glial sheath advances, the native circuitry is disrupted, and the loss of inhibitory interneurons may cause this phenomena.

L1 Modification

SNR(Burst Trial)	0.03				
LFP	0.18	0.7			
FR% Change Single Shot	0.004	0.41	0.02		
Channel Response to Single Shot	0.16	0.16	0.1	0.002	
Channel Response to Burst Shot	0.57	0.58	0.79	0.06	0.07
	SNR(Single Trial)	SNR(Burst Trial)	LFP	FR% Change Single Shot	Channel Response to Single Shot

Unmodified

SNR(Burst Trial)	0.5				
LFP	0.49	0.94			
FR% Change Single Shot	0.68	0.56	0.53		
Channel Response to Single Shot	0.62	0.34	0.4	0.01	
Channel Response to Burst Shot	0.16	0.005	0.99	0.14	0.03
	SNR(Single Trial)	SNR(Burst Trial)	LFP	FR% Change Single Shot	Channel Response to Single Shot

Figure 31: Correlations of Different Measured Parameters by Experimental Group. Yellow indicates significance found through multiway ANOVA at a level of $p < 0.1$. The small sample size made it difficult to find significant correlations, so a higher p value was used for this comparison.

The correlation between the number of channels detected to be responding and the firing rate percent change is expected, as the detection of response depends on a firing rate threshold. The correlation between the number of channels that respond to a burst shot and the number of channels that respond to a single shot is also expected. The unmodified probe showed a significant correlation between the SNR of the spikes in the burst trial and the number of channels responding to the burst shot. This was an expected result, however, it was not reflected in the L1 data, Conversely, the L1 probes showed a significant correlation between the percent change in firing rate for a single shot trial and the SNR for that trial, while the unmodified probes did not. SNR is based on the quality of the neural snippets, and the location of the implant plays a major role in the number of channels responding, so there is no direct anatomical relationship between these two parameters. However, we would expect that as the sample size increases, the number of channels that respond and the SNR will be correlated for both types of stimulation.

The LFP peak to peak amplitude measurement is taken from a spontaneous trial, so it is considered to reflect the health of the cortex rather than the strength of the LFP response, In the L1 probes this measurement was correlated with the number of channels responding to single shot, but not in the unmodified probes. The lack of correlation in the unmodified probes may be due to poor recording quality and the inability to collect enough responses for the correlation to be significant.

The statistical significant values rely on the assumption that all 16 channels of the Michigan probe are independent samples. This is a questionable assumption because of the common location of all sites on the same shank. Future studies will test these trends with FMA electrodes where each individual site is physically isolated from the others.

6.4 CHARACTERISTIC TIME COURSE

A multiway analysis of variance (ANOVA) was performed to quantify the degree of signal change over time. In most cases the number of samples was too low for apparent differences in the data to be considered statistically significant. However, there was a significant difference of $p = 0.075$ between the SNR for the burst trials in weeks 4 and week 8. (Figure 10) Also, the week 3 LFP peak to peak amplitude was significantly higher than all other weeks except week 4, and week 4 was higher than weeks 1, 2, 5, and 8. ($p = 0.05$, Figure 11) Although the correlation coefficients suggest only weak correlation, this provides some insight into the time-course of signal quality. There is a brief period of improvement between the time of the surgery and weeks 2 and 3. We attribute this improvement to the healing of the implant site and the initial recovery and stabilization of the tissue. The best recording window tends to occur from about week 2 to week 4. After weeks 3 to 4 the slower reaction typical of chronic gliosis begins to reduce the ability of the probe to record useful signal, and by week 8 some types of evoked signal in the unmodified probes were lost altogether.

6.5 L1 VS. UNMODIFIED COMPARISON

Initial results suggest that L1 coated probes will be susceptible to the general same time-course of signal quality as unmodified probes. It is expected that there will be improvement during initial healing, and then moderate reduction in signal quality as the tissue forms a more permanent scar structure. L1 was shown to demonstrate increased neuronal cell density in-vitro. [31] From this we would expect a higher density of neurons in the immediate area of the probe in

an *in-vivo* model. Such a result would, as our data suggest, result in larger waveforms, and possibly an increase in the dimensionality of the information that could be carried. It also appears that L1 may decrease the slope of the 4 to 8 week decline phase in the number of channels that give an evoked response, and cause the implant to ultimately plateau at a higher level of performance. L1 has been shown to demonstrate increased neuronal cell density *in-vitro*, and the stronger SNR of the L1-coated probes in some trials suggests the possibility of neurons migrating in the direction of the probe. [31] Some of the parameters that were measured did not show any trends between the two coatings. It is too early in the study to conclude whether this means that the glial sheath is not being affected. Future analysis will consider this trend in greater detail. From this we would expect a higher density of neurons in the immediate area of the probe in an *in-vivo* model. Such a result would, as our data suggests, result in better SNR and possibly an increase in the dimensionality of the information that could be carried.

6.6 CONCLUSIONS

Several parameters characterizing the quality of the neural signal were characterized over time. We were unable to reliably measure impedance in our current mode. The SNR of the single shot trials improves as the acute responses heals, then decreases for the remainder of the life of the probe. The peak to peak amplitude of spontaneous LFP follows a similar trend, increasing for about two weeks, and then decreasing steadily. On the unmodified probes, the number of channels responding to stimulation decreased with time, especially after 6 weeks. The L1

appeared to show evoked responses longer, but that data was not significant. The LFP was inconsistent in both types of stimulation trials.

Two of the major mechanisms believed to contribute to chronic electrode failure are the formation of the glial sheath around the electrode and the decrease of neuronal cell density result in a kill zone. The larger SNR of the waveform data, in combination with the stronger stimulus response in the single shot stimulus and the LFP PPA suggest that the L1 modified probes exhibit a higher neuronal cell density in the area surrounding the electrode than the control probes.

APPENDIX A

ADDITIONAL PLOTS FOR WAVEFORM ANALYSIS

Many of the graphs presented are highly processed information and much of the data behind them is hidden. This appendix provides several examples of lower level plots from different subjects, displaying a wider variety of less processed data, as well as some examples of alternative parameters.

A.1 WAVEFORM PSTH EXAMPLES

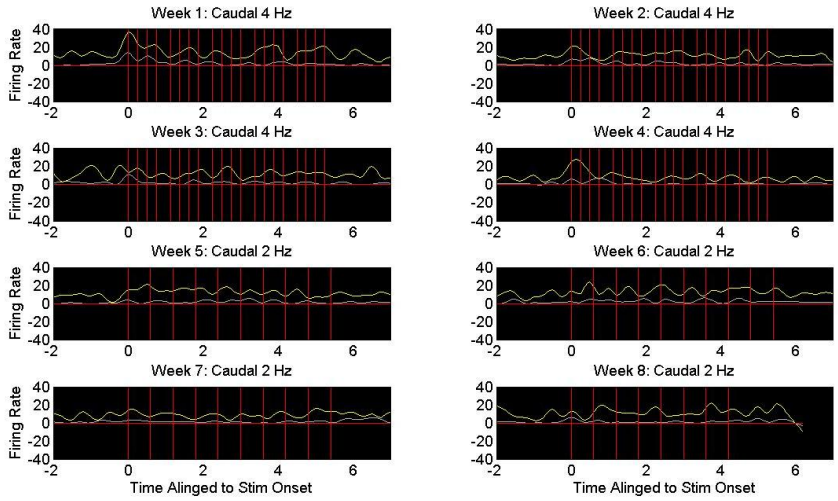

Figure A1.1 L1 (Rat 1) Burst Stimulation over 8 weeks. The experiment was changed from 4 Hz to 2 Hz at week 5 to increase the contrast between the different frequencies. 500 ms bins are used for clarity.

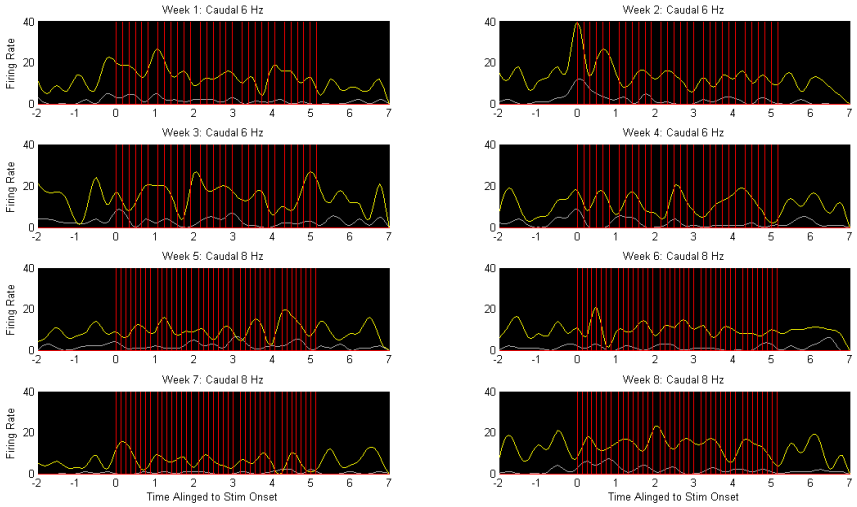

Figure A1.2 L1 (Rat 1) Burst Stimulation over 8 weeks. The experiment was changed from 6 Hz to 8 Hz at week 5 to increase the contrast between the different frequencies. 500 ms bins

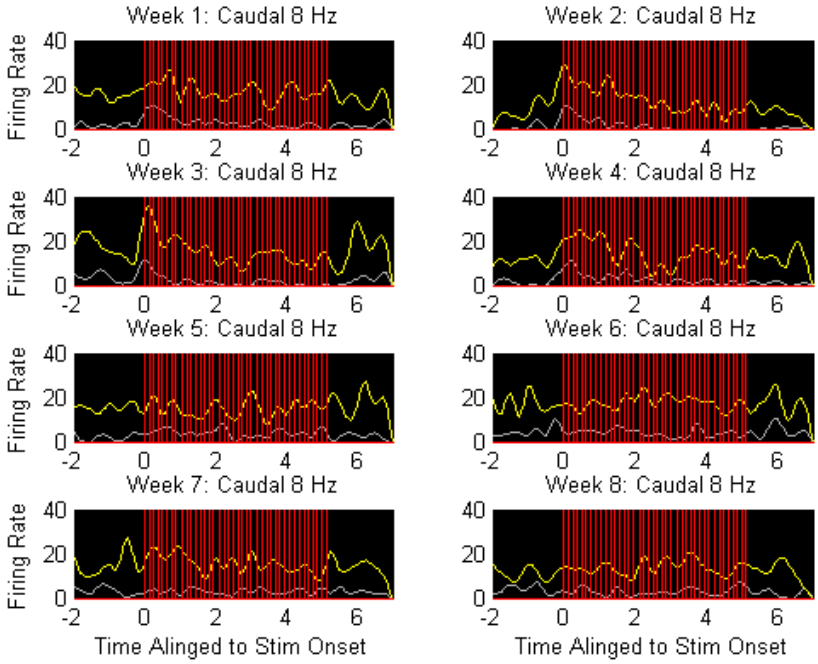

Figure A1.3. Unmodified Rat 1 High Frequency over 8 weeks.

A.2 STABILITY PSTH PLOTS

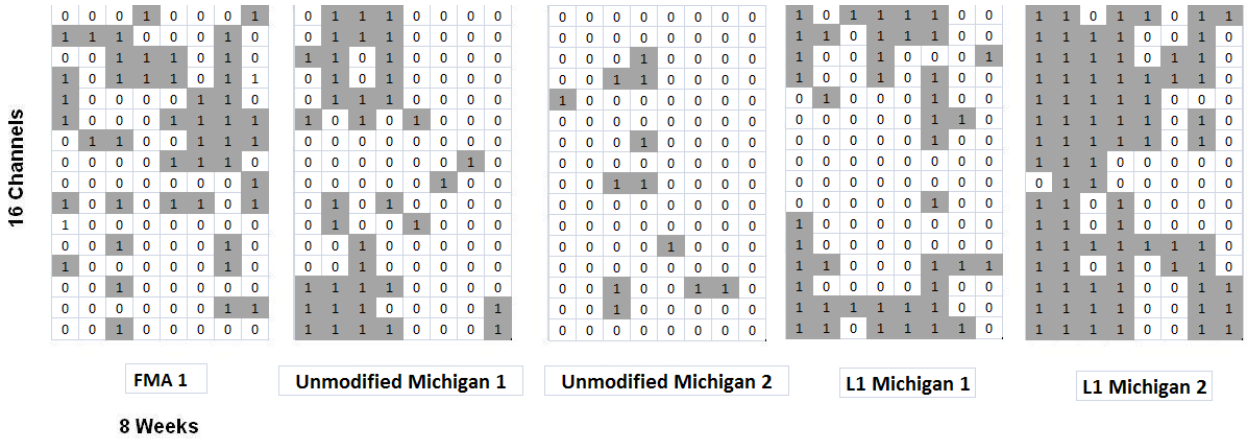

Figure A2.1 Grey indicates a channel that responds to the single shot stimulus. White indicates a silent channel.

Figure A2.1 provides a qualitative estimation of the consistency of channels responding over time. If a channel were consistent, it would show the same response following from left to right.

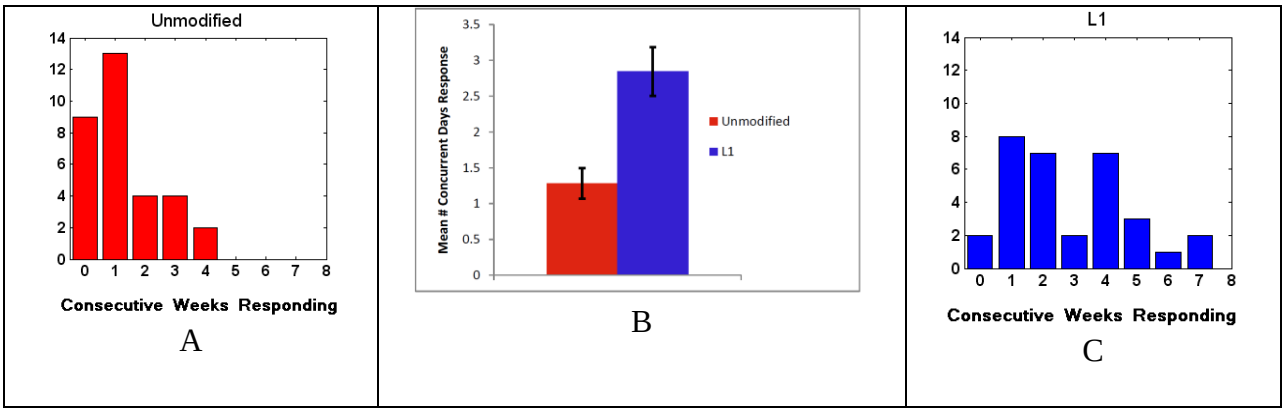

Figure A2.2 The longest continues strech of days in which a response could be detected was counted for each channel. (A) Histogram of the longest consequtive responses for the unmodified probe. (B) Mean and SEM of probes by experimental group. n = 32, A Student's t-test comparing the two groups was significant at $p = 0.05$. (C) Histogram of the longest consequtive responses for the L1 probe.

APPENDIX B

EXPLANATION OF SPIKE SELECTION ALGORITHM

In order to increase consistency between weekly recordings, it was decided to use a custom written Matlab program to isolate neural spikes from the data stream. The method of selecting which waveforms are extracted from the data stream as neural spiking events is an important component of the high frequency waveform analysis. The algorithm used becomes significantly more important when noise levels are high and it is more difficult to isolate spiking events.

B.1 SPIKE THRESHOLDING

The raw 25 kHz data stream from the RX5 was loaded into Matlab. A band-pass filter from 300 Hz to 3000 Hz was applied. A custom threshold for each day was set by taking a proportion of the RMS value of the signal. The threshold was then manually adjusted to until the data showed a roughly estimated baseline firing rate. The quality of the appearance of the waveforms was used as a secondary criterion for determining the correct threshold level.

Once the threshold was determined, the spikes were selected based criterion for crossing the threshold. Candidate threshold passings were identified whenever the data stream crossed the threshold. However, in order to be characterized as a spike it was required that the signal also return back below the threshold within 50 samples, which corresponds to about 2 milliseconds. It was required that there be a minimum of 100 samples (4ms) between spiking events. This forces an arbitrary theoretical firing rate maximum of 250 Hz, however, we find that our firing rates were computed about an order of magnitude lower than this theoretical maximum value. Spikes located less than a full spike width from either the start of the end of a recording were eliminated.

The ability to manually tune the threshold up or down is a key improvement over the software package (Open Sorter) provided by Tucker Davis Technologies. Depending on the signal to noise ratio of any given recording, the window of successful spike detection can be only a few micro volts wide. Any deviations that occur during a recording procedure can result in selecting noise, or losing the signal. The offline analysis provided by our Matlab program controls for this problem.

B.2 SPIKE SORTING

A template sorting algorithm was used to assist the researcher in sorting the spikes by candidate waveforms. Because of the problems with the Michigan probe reference, we were unable to reliably isolate more than one waveform category. The algorithm computes the mean of all waveforms, then creates a window of 2.5 standard deviations above and below this mean, and

classifies all waveforms that fall do not leave this window as a snip group 1. Any snips that leave this window are considered unsorted. The Matlab program displayed in Figure B1.1 is then used to visually inspect the sort, and corrections are made manually.

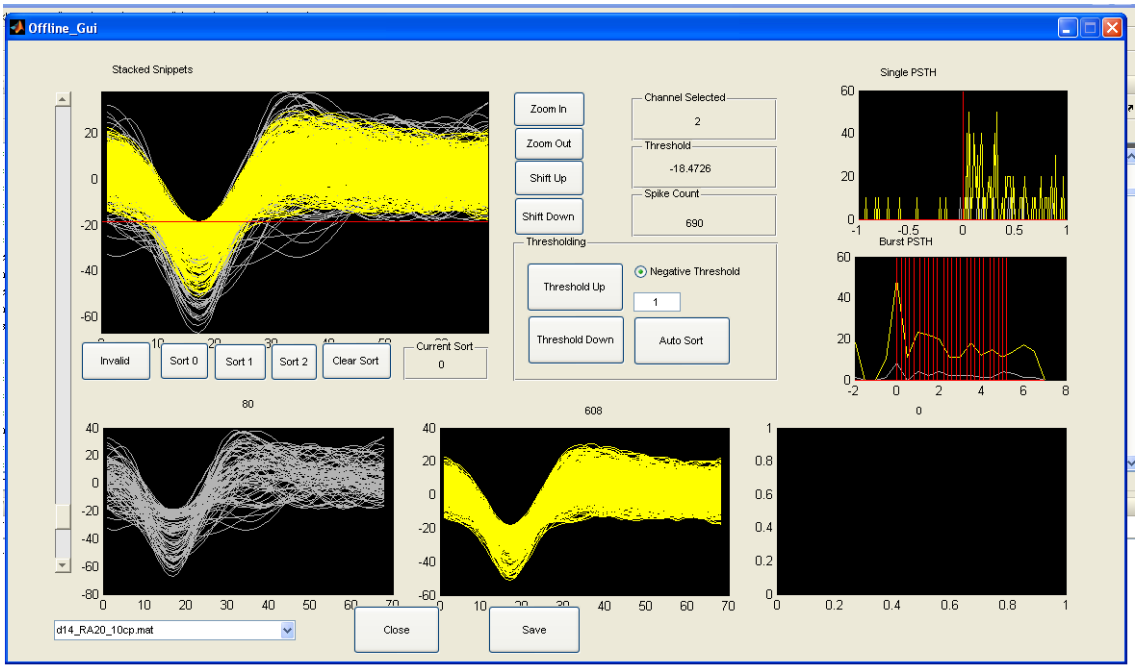

Figure B1.1 Example of the custom Matlab program used to sort spikes into waveform category.

The PSTH of both the single shot PSTH and the Burst PSTH are shown on the right. The stacked waveform plot is displayed, as well as the plots of up to 3 units and the number of spike in each category.

APPENDIX C

L1 COATING MODIFICATION METHODS

One shank sixteen channel chronic silicon probes from NeuroNexus Technologies (Ann Arbor, MI) were chosen to be used during this study. The design and fabrication of these probes has been published elsewhere. [52] L1 was immobilized on the surface of the probes using silane chemistry. Silane chemistry allows surface patterning and immobilization of proteins or peptides on silicon substrates through hetero-bifunctional cross-linking reagent, 4-maleimidobutyric acid N-hydroxysuccinimide ester (GMBS). [53] Poly(ethylene glycol)-NH2 (PEG-NH2) was added after L1 immobilization, to block the remaining reactive GMBS groups and to inhibit non-specific protein adsorption to the surface. [31]

The surface modification was performed using an experimental procedure similar to those previously reported. [52, 53] Briefly, after cleaning and hydroxylation with HNO3, the probes were carefully immersed in a 2% solution of (3-mercaptopropyl) trimethoxysilane (MTS) (Sigma-Aldrich, MO, USA) and treated for 1 hour with 2 mM of GMBS (Sigma-Aldrich). L1 (100 µg/ml) was applied for 1 hour at 4oC on the GMBS treated probe surface. The L1 immobilized probes were rinsed with phosphate buffered saline (PBS) (pH 7.4), and treated with 100 µM mPEG-NH2 (Nektar, CA) solution for 30 min to cap the rest of the active NHS ester

groups of the GMBS biomolecule. The probes were implanted in the animals immediately after this process.

APPENDIX D

FURTHER EXAMPLES OF BURST RESPONSES

The burst response is the most complicated level of signal decoding presented. Additional examples of the differentiation between different types of response are presented.

D.1 WAVEFORM EXAMPLES

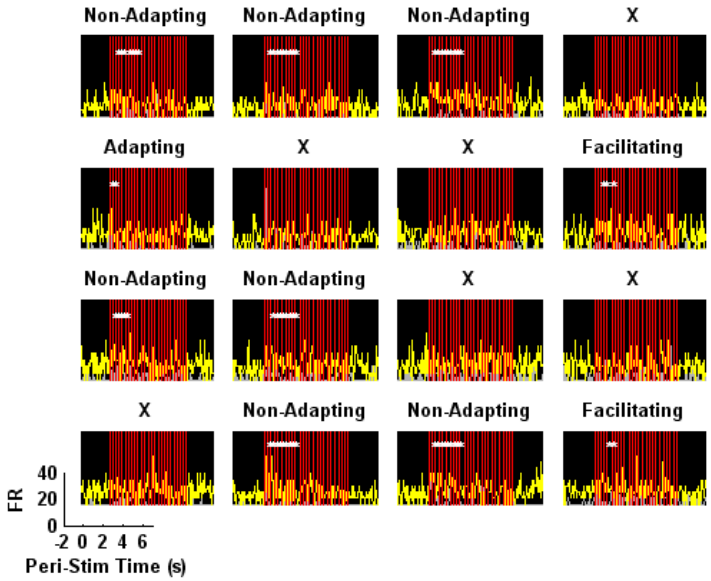

Figure D1.1: Week 1, Unmodified Michigan, 5 Hz Stimulation, white * indicates the front end of a window containing a significant response. All windows start at time = 0

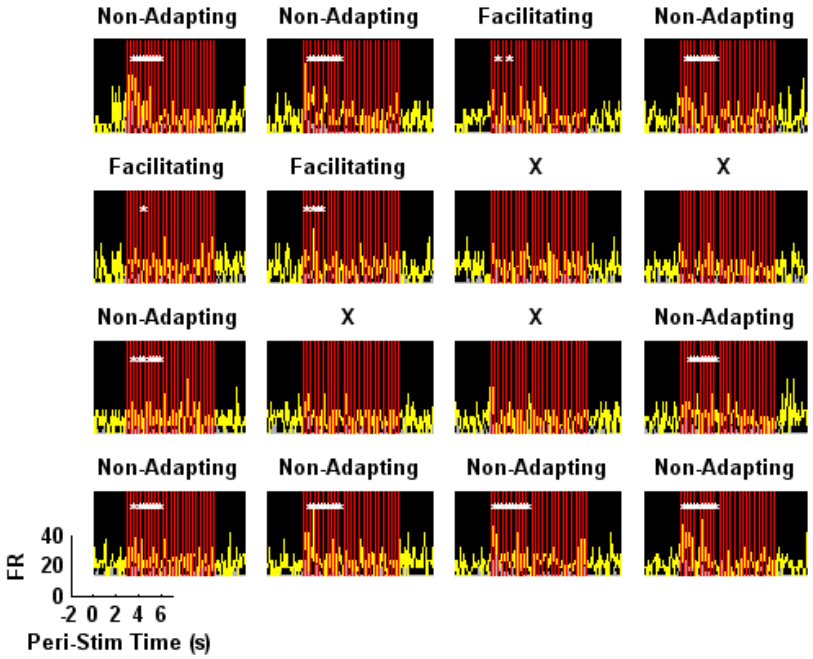

Figure D1.2 Week 2, Unmodified Michigan, 5 Hz Stimulation

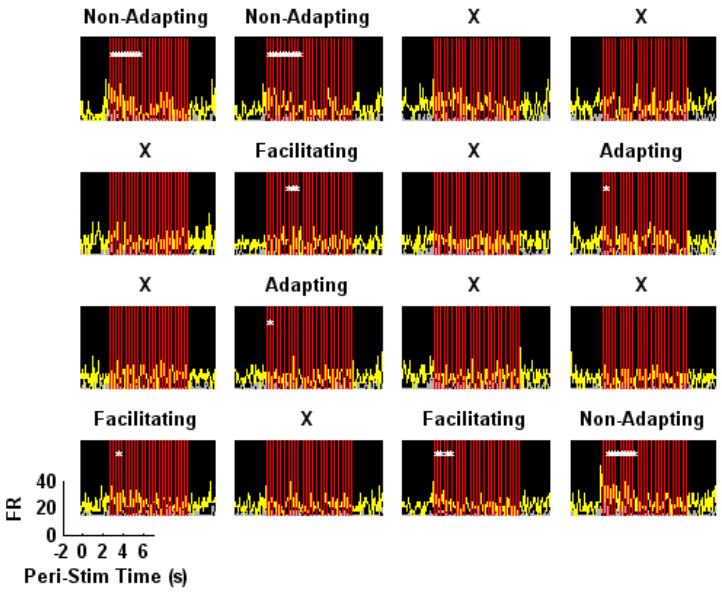

Figure D1.3 Week 3, Unmodified Michigan, 5 Hz Stimulation

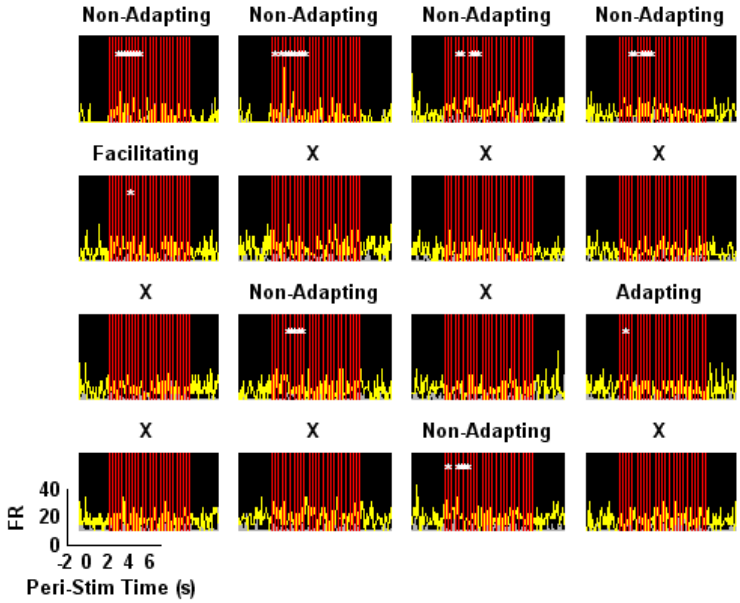

Figure D1.4 Week 4, Unmodified Michigan, 5 Hz Stimulation

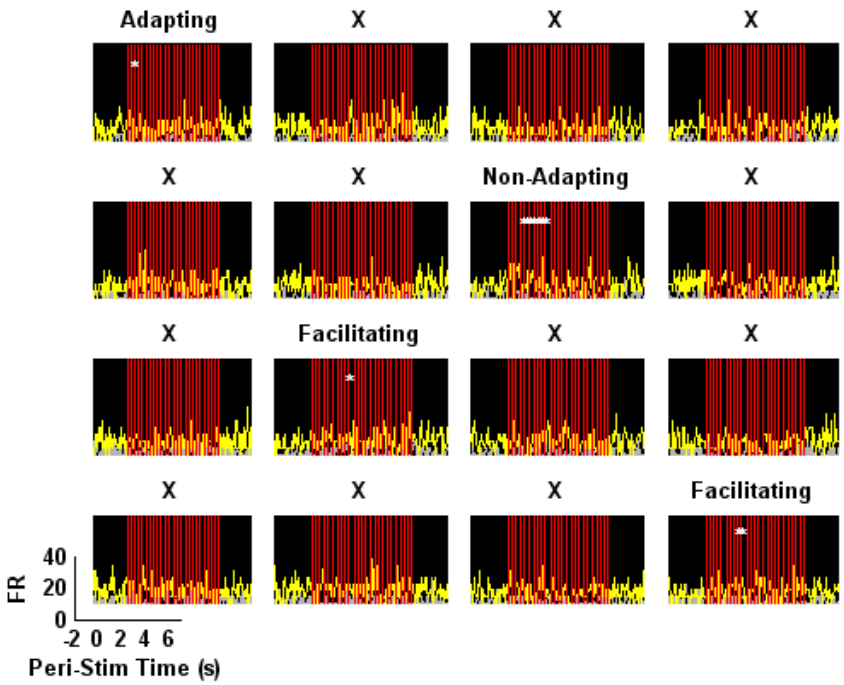

Figure D1.5 Week 5, Unmodified Michigan, 5 Hz Stimulation

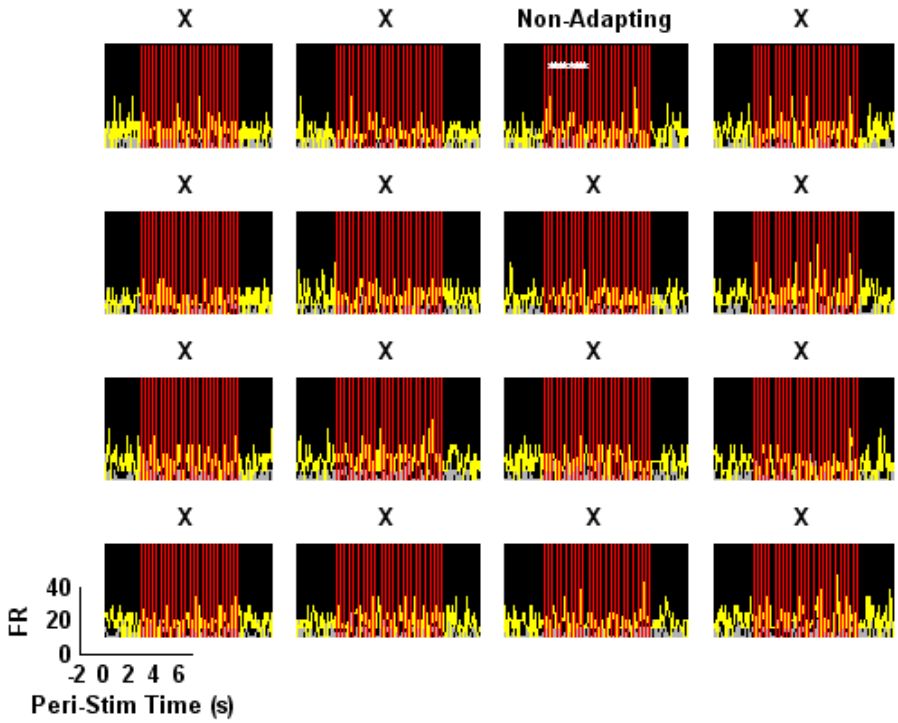

Figure D1.6 Week 6, Unmodified Michigan, 5 Hz Stimulation

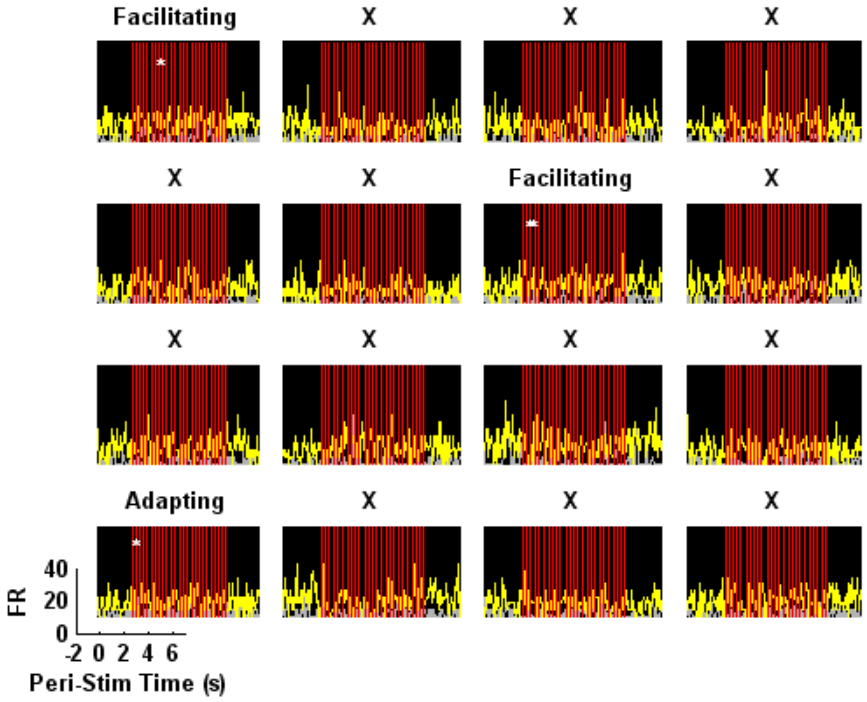

Figure D1.7 Week 7, Unmodified Michigan, 5 Hz Stimulation

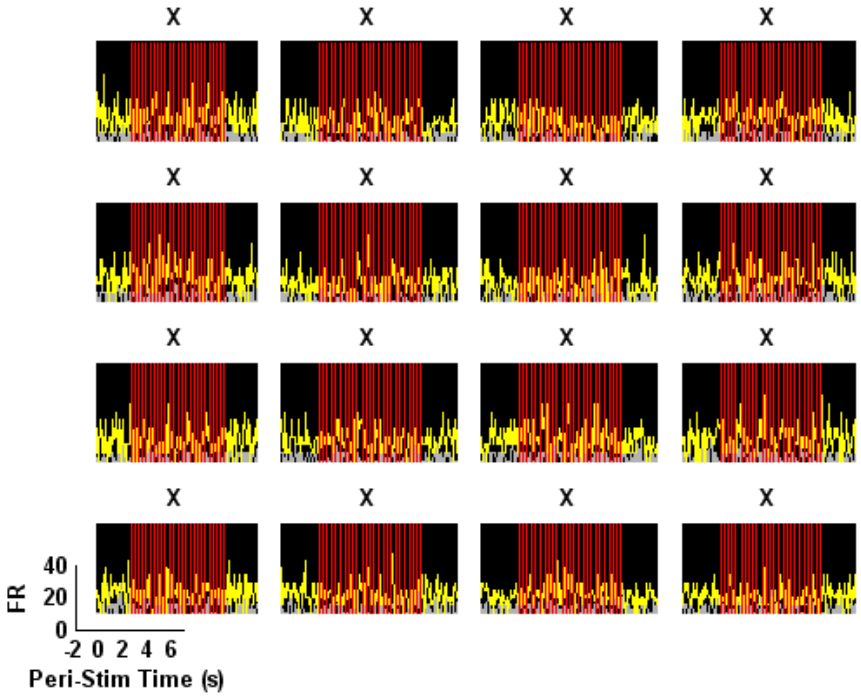

Figure D1.8 Week 8, Unmodified Michigan, 5 Hz Stimulation

D.2 LFP EXAMPLES

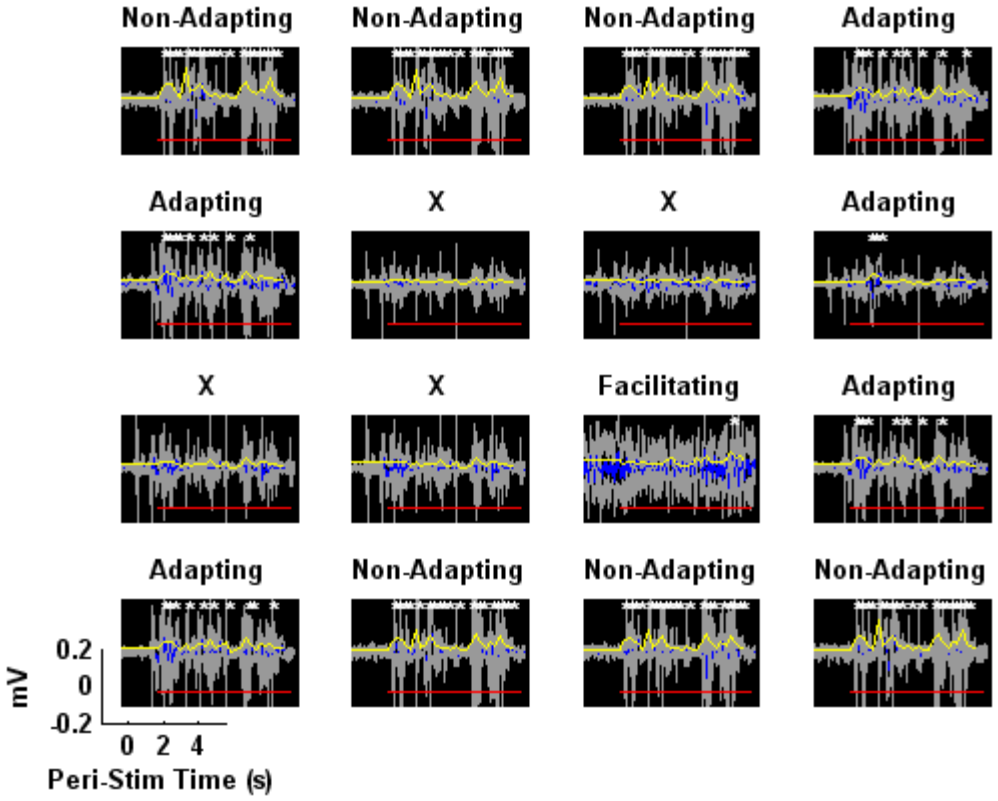

Figure D2.1 Week 1, Unmodified Michigan, 5 Hz Stimulation. Yellow indicates the rms value of the trace, white indicates a window that showed at least a 2x increase relative to the pre-stim value. The red line indicates the presence of the stimulus.

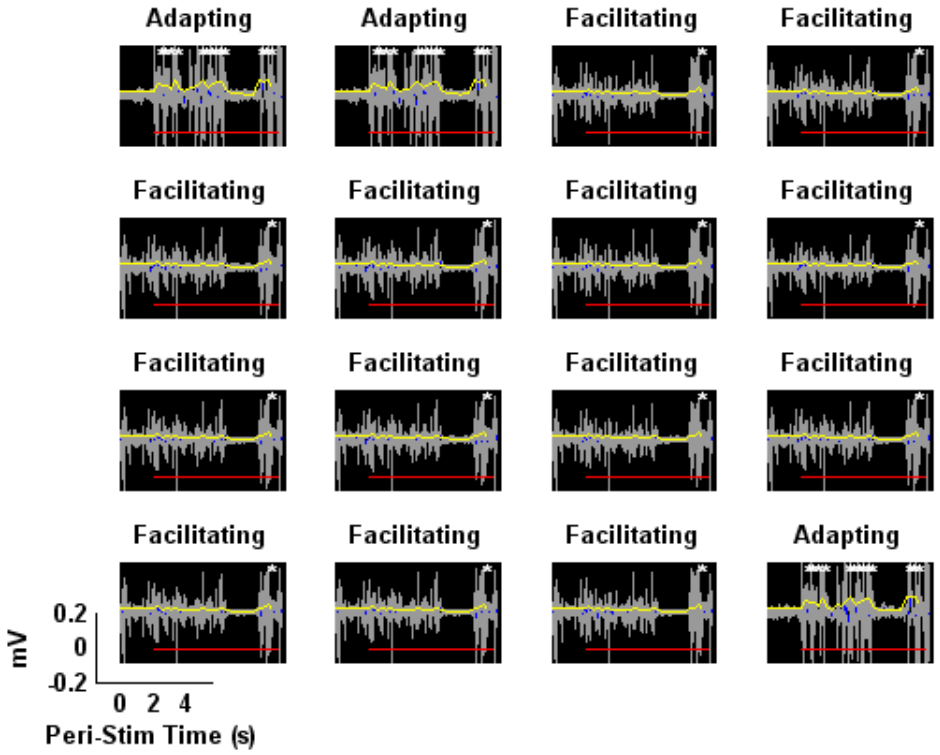

Figure D2.2 Week 2, Unmodified Michigan, 5 Hz Stimulation

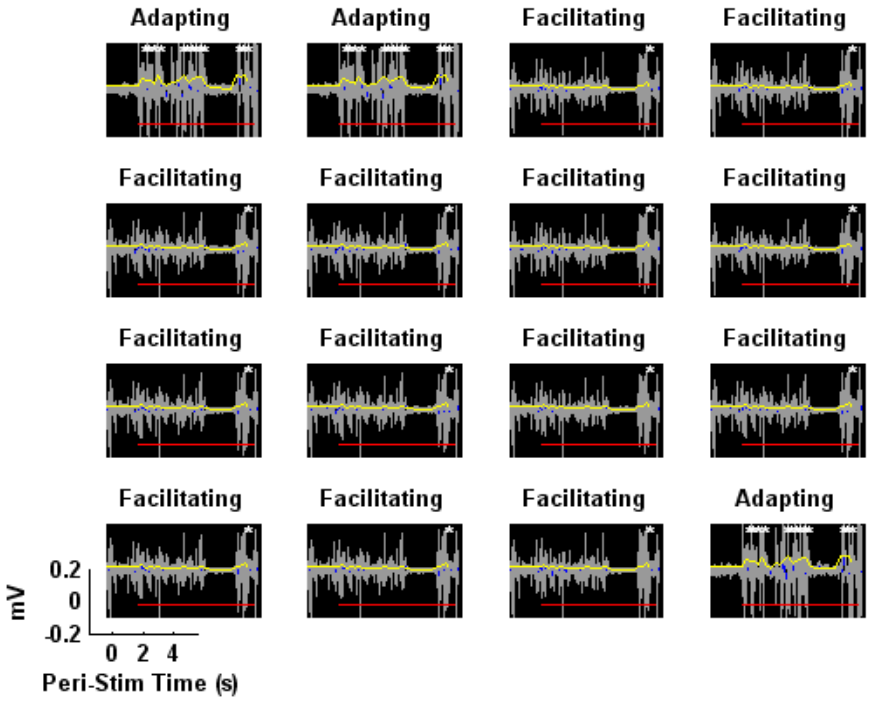

Figure D2.3 Week 3, Unmodified Michigan, 5 Hz Stimulation

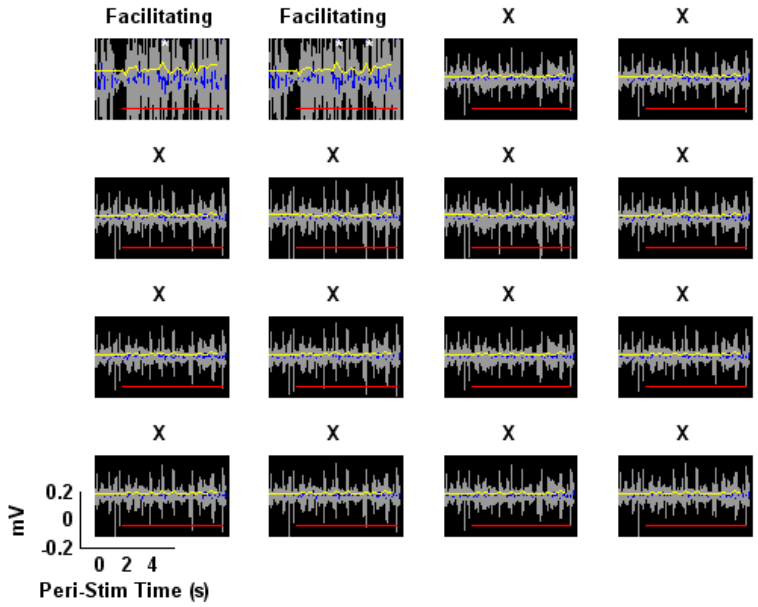

Figure D2.4 Week 4, Unmodified Michigan, 5 Hz Stimulation

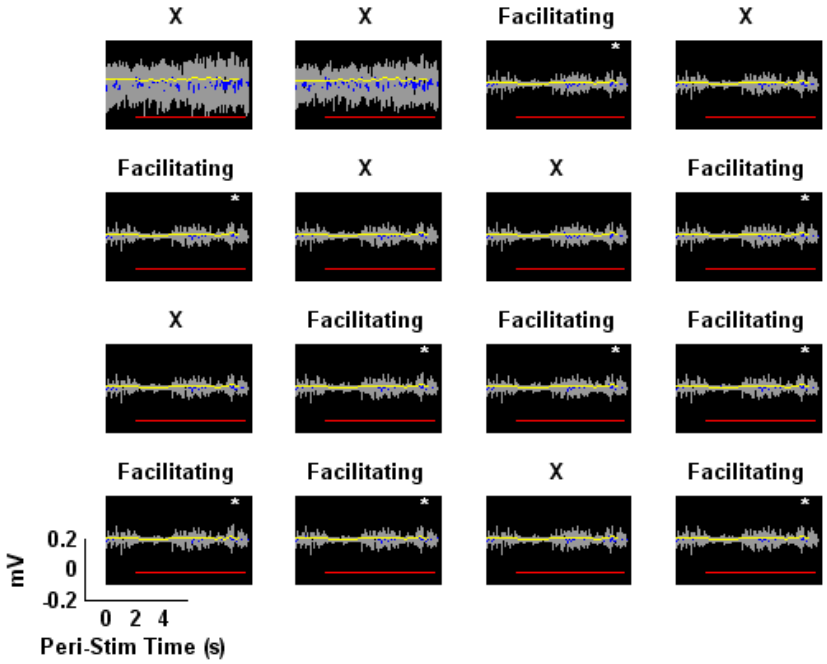

Figure D2.5 Week 5, Unmodified Michigan, 5 Hz Stimulation

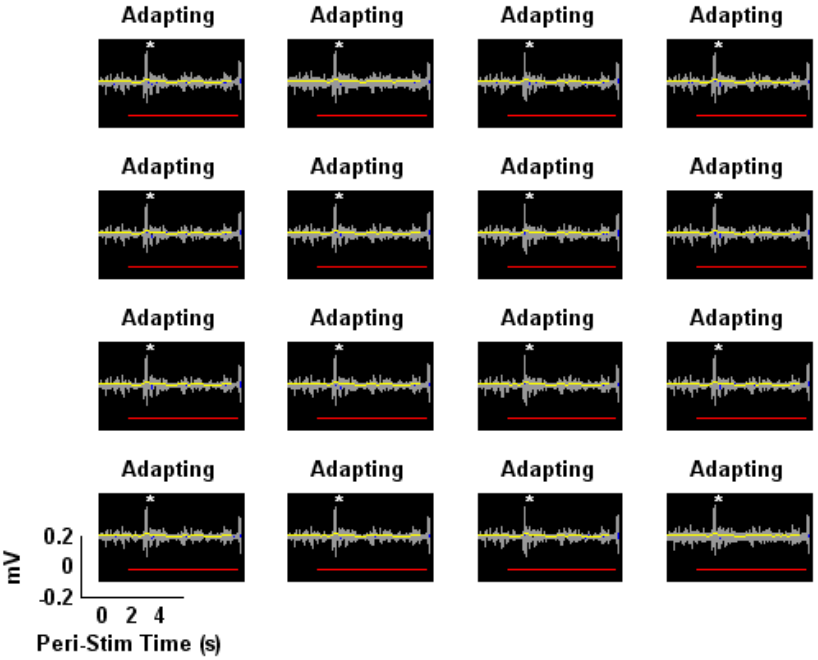

Figure D2.6 Week 6, Unmodified Michigan, 5 Hz Stimulation

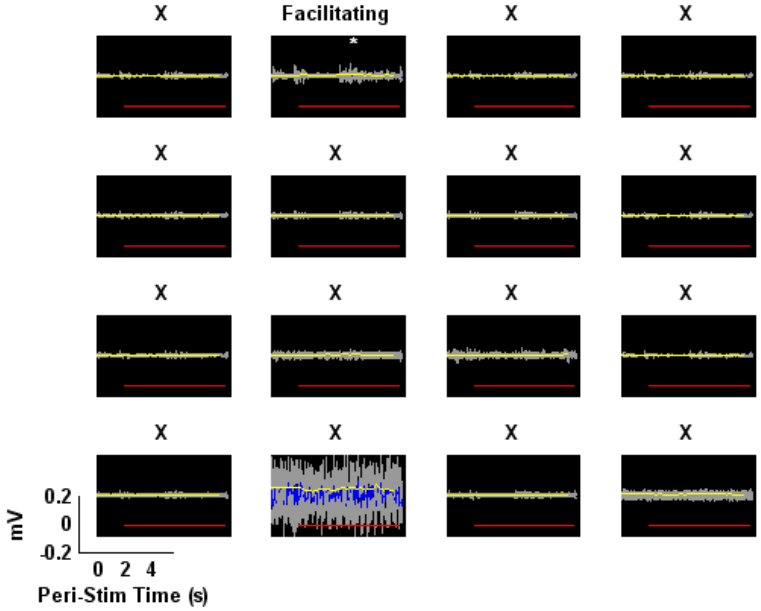

Figure D2.7 Week 7, Unmodified Michigan, 5 Hz Stimulation

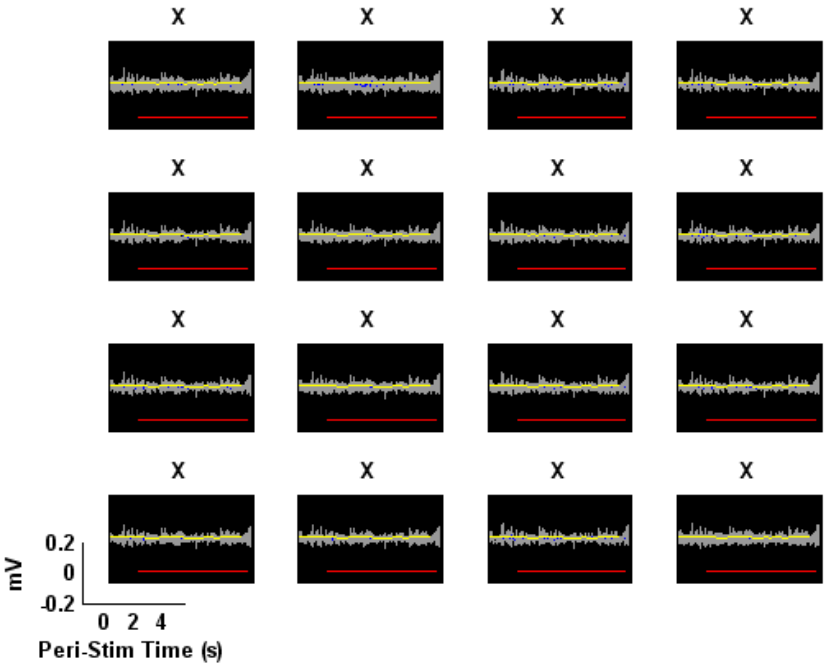

Figure D2.8 Week 8, Unmodified Michigan, 5 Hz Stimulation

BIBLIOGRAPHY

1. Velliste, M., et al., *Cortical control of a prosthetic arm for self-feeding.* Nature, 2008. **453**(7198): p. 1098-101.

2. Schwartz, A.B., et al., *Brain-controlled interfaces: movement restoration with neural prosthetics.* Neuron, 2006. **52**(1): p. 205-20.

3. Schwartz, A.B., *Cortical neural prosthetics.* Annu Rev Neurosci, 2004. **27**: p. 487-507.
4. Kennedy, P.R., et al., *Direct control of a computer from the human central nervous system.* IEEE Trans Rehabil Eng, 2000. **8**(2): p. 198-202.

5. Purcell, E.K., et al., *Flavopiridol reduces the impedance of neural prostheses in vivo without affecting recording quality.* J Neurosci Methods, 2009. **183**(2): p. 149-57.

6. Williams, J.C., et al., *Complex impedance spectroscopy for monitoring tissue responses to inserted neural implants.* J Neural Eng, 2007. **4**(4): p. 410-23.

7. Ludwig, K.A., et al., *Chronic neural recordings using silicon microelectrode arrays electrochemically deposited with a poly(3,4-ethylenedioxythiophene) (PEDOT) film.* J Neural Eng, 2006. **3**(1): p. 59-70.

8. Cheung, K.C., *Implantable microscale neural interfaces.* Biomed Microdevices, 2007. **9**(6): p. 923-38.

9. Jones, K.E., P.K. Campbell, and R.A. Normann, *A glass/silicon composite intracortical electrode array.* Ann Biomed Eng, 1992. **20**(4): p. 423-37.

10. Kipke, D.R., et al., *Silicon-substrate intracortical microelectrode arrays for long-term recording of neuronal spike activity in cerebral cortex.* IEEE Trans Neural Syst Rehabil Eng, 2003. **11**(2): p. 151-5.

11. Nicolelis, M.A., et al., *Chronic, multisite, multielectrode recordings in macaque monkeys.* Proc Natl Acad Sci U S A, 2003. **100**(19): p. 11041-6.

12. Rousche, P.J. and R.A. Normann, *Chronic recording capability of the Utah Intracortical Electrode Array in cat sensory cortex.* J Neurosci Methods, 1998. **82**(1): p. 1-15.

13. Polikov, V.S., P.A. Tresco, and W.M. Reichert, *Response of brain tissue to chronically implanted neural electrodes.* J Neurosci Methods, 2005. **148**(1): p. 1-18.

14. Szarowski, D.H., et al., *Brain responses to micro-machined silicon devices.* Brain Res, 2003. **983**(1-2): p. 23-35.

15. Chabot, S., G. Williams, and V.W. Yong, *Microglial production of TNF-alpha is induced by activated T lymphocytes. Involvement of VLA-4 and inhibition by interferonbeta-1b.* J Clin Invest, 1997. **100**(3): p. 604-12.

16. Biran, R., D.C. Martin, and P.A. Tresco, *Neuronal cell loss accompanies the brain tissue response to chronically implanted silicon microelectrode arrays.* Exp Neurol, 2005. **195**(1): p. 115-26.

17. Grill, W.M. and J.T. Mortimer, *Electrical properties of implant encapsulation tissue.* Ann Biomed Eng, 1994. **22**(1): p. 23-33.

18. Merrill, D.R. and P.A. Tresco, *Impedance characterization of microarray recording electrodes in vitro.* IEEE Trans Biomed Eng, 2005. **52**(11): p. 1960-5.

19. Liu, X., et al., *Stability of the interface between neural tissue and chronically implanted intracortical microelectrodes.* IEEE Trans Rehabil Eng, 1999. **7**(3): p. 315-26.

20. Williams, J.C., R.L. Rennaker, and D.R. Kipke, *Long-term neural recording characteristics of wire microelectrode arrays implanted in cerebral cortex.* Brain Res Brain Res Protoc, 1999. **4**(3): p. 303-13.

21. Cui, X., et al., *Surface modification of neural recording electrodes with conducting polymer/biomolecule blends.* J Biomed Mater Res, 2001. **56**(2): p. 261-72.

22. Massia, S.P., M.M. Holecko, and G.R. Ehteshami, *In vitro assessment of bioactive coatings for neural implant applications.* J Biomed Mater Res A, 2004. **68**(1): p. 177-86.

23. He, W. and R.V. Bellamkonda, *Nanoscale neuro-integrative coatings for neural implants.* Biomaterials, 2005. **26**(16): p. 2983-90.

24. Wadhwa, R., C.F. Lagenaur, and X.T. Cui, *Electrochemically controlled release of dexamethasone from conducting polymer polypyrrole coated electrode.* J Control Release, 2006. **110**(3): p. 531-41.

25. Leprince, L., et al., *Dexamethasone electrically controlled release from polypyrrole-coated nanostructured electrodes.* J Mater Sci Mater Med, 2010. **21**(3): p. 925-30.

26. Otto, K.J., M.D. Johnson, and D.R. Kipke, *Voltage pulses change neural interface properties and improve unit recordings with chronically implanted microelectrodes.* IEEE Trans Biomed Eng, 2006. **53**(2): p. 333-40.

27. Johnson, M.D., et al., *Bias voltages at microelectrodes change neural interface properties in vivo.* Conf Proc IEEE Eng Med Biol Soc, 2004. **6**: p. 4103-6.

28. McConnell, G.C., R.J. Butera, and R.V. Bellamkonda, *Bioimpedance modeling to monitor astrocytic response to chronically implanted electrodes.* J Neural Eng, 2009. **6**(5): p. 055005.

29. McAdams, E.T. and J. Jossinet, *Tissue impedance: a historical overview.* Physiol Meas, 1995. **16**(3 Suppl A): p. A1-13.

30. Halter, R.J., et al., *Genetic and least squares algorithms for estimating spectral EIS parameters of prostatic tissues.* Physiol Meas, 2008. **29**(6): p. S111-23.

31. Azemi, E., et al., *Surface immobilization of neural adhesion molecule L1 for improving the biocompatibility of chronic neural probes: In vitro characterization.* Acta Biomater, 2008. **4**(5): p. 1208-17.

32. Petersen, C.C., A. Grinvald, and B. Sakmann, *Spatiotemporal dynamics of sensory responses in layer 2/3 of rat barrel cortex measured in vivo by voltage-sensitive dye imaging combined with whole-cell voltage recordings and neuron reconstructions.* J Neurosci, 2003. **23**(4): p. 1298-309.

33. Petersen, C.C., *The functional organization of the barrel cortex.* Neuron, 2007. **56**(2): p. 339-55.

34. Aronoff, R. and C.C. Petersen, *Layer, column and cell-type specific genetic manipulation in mouse barrel cortex.* Front Neurosci, 2008. **2**(1): p. 64-71.

35. Yu, C., et al., *Parallel thalamic pathways for whisking and touch signals in the rat.* PLoS Biol, 2006. **4**(5): p. e124.

36. Bokor, H., L. Acsady, and M. Deschenes, *Vibrissal responses of thalamic cells that project to the septal columns of the barrel cortex and to the second somatosensory area.* J Neurosci, 2008. **28**(20): p. 5169-77.

37. Brecht, M., *Barrel cortex and whisker-mediated behaviors.* Curr Opin Neurobiol, 2007. **17**(4): p. 408-16.

38. Schubert, D., R. Kotter, and J.F. Staiger, *Mapping functional connectivity in barrel-related columns reveals layer- and cell type-specific microcircuits.* Brain Struct Funct, 2007. **212**(2): p. 107-19.

39. Pierret, T., P. Lavallee, and M. Deschenes, *Parallel streams for the relay of vibrissal information through thalamic barreloids.* J Neurosci, 2000. **20**(19): p. 7455-62.

40. Simons, D.J. and T.A. Woolsey, *Morphology of Golgi-Cox-impregnated barrel neurons in rat SmI cortex.* J Comp Neurol, 1984. **230**(1): p. 119-32.

41. Krupa, D.J., et al., *Layer-specific somatosensory cortical activation during active tactile discrimination.* Science, 2004. **304**(5679): p. 1989-92.

42. Alloway, K.D., *Information processing streams in rodent barrel cortex: the differential functions of barrel and septal circuits.* Cereb Cortex, 2008. **18**(5): p. 979-89.

43. Vetter, R.J., et al., *Chronic neural recording using silicon-substrate microelectrode arrays implanted in cerebral cortex.* IEEE Trans Biomed Eng, 2004. **51**(6): p. 896-904.

44. Webb, K., et al., *Substrate-bound human recombinant L1 selectively promotes neuronal attachment and outgrowth in the presence of astrocytes and fibroblasts.* Biomaterials, 2001. **22**(10): p. 1017-28.

45. Lemmon, V., et al., *Neurite growth on different substrates: permissive versus instructive influences and the role of adhesive strength.* J Neurosci, 1992. **12**(3): p. 818-26.

46. Kenwrick, S., A. Watkins, and E. De Angelis, *Neural cell recognition molecule L1: relating biological complexity to human disease mutations.* Hum Mol Genet, 2000. **9**(6): p. 879-86.

47. Hortsch, M., *The L1 family of neural cell adhesion molecules: old proteins performing new tricks.* Neuron, 1996. **17**(4): p. 587-93.

48. Dihne, M., et al., *A new role for the cell adhesion molecule L1 in neural precursor cell proliferation, differentiation, and transmitter-specific subtype generation.* J Neurosci, 2003. **23**(16): p. 6638-50.

49. Hayton, S.M., A. Kriss, and D.P. Muller, *Comparison of the effects of four anaesthetic agents on somatosensory evoked potentials in the rat.* Lab Anim, 1999. **33**(3): p. 243-51.

50. Wolfe, J., et al., *Texture coding in the rat whisker system: slip-stick versus differential resonance.* PLoS Biol, 2008. **6**(8): p. e215.

51. Temereanca, S., E.N. Brown, and D.J. Simons, *Rapid changes in thalamic firing synchrony during repetitive whisker stimulation.* J Neurosci, 2008. **28**(44): p. 11153-64.

52. Drake, K.L., et al., *Performance of planar multisite microprobes in recording extracellular single-unit intracortical activity.* IEEE Trans Biomed Eng, 1988. **35**(9): p. 719-32.

53. Bhatia, S.K., et al., *Use of thiol-terminal silanes and heterobifunctional crosslinkers for immobilization of antibodies on silica surfaces.* Anal Biochem, 1989. **178**(2): p. 408-13.